Phenomenological model of the copper oxide superconductors

R. A. Klemm*
Ames Laboratory and Department of Physics, Iowa State University, Ames, Iowa 50011
(Received 3 January 1989; revised manuscript received 8 August 1989)

We propose a phenomenological model for the copper oxide superconductors in which one complex s-wave order parameter (OP) is associated with each of the N conducting layers per unit cell, with $N-1$ equal spacings d and one different spacing d'; the c axis repeat distance $s=d'+(N-1)d$. The layers are coupled by Josephson-like tunneling, with parameters ζ_1 and ζ_2, respectively. The Gaussian fluctuation free energy is diagonalized, yielding N distinct T_c values. Just above the highest T_c, the fluctuations are usually dominated by the three-dimensional (3D) regime of a single cellular OP. In the 2D regime further above T_c, more of the OP's contribute to the fluctuations, their relative contributions depending upon the ζ_1 and ζ_2 values. The temperature (T) and angular (θ) dependence of the resulting fluctuation magnetization $\mathbf{M}(\theta,T)$ is calculated. In a weak magnetic field $\mathbf{B}$ [$B<B_0=\phi_0/(sv_F\tau_\phi)$, where ϕ_0, v_F, and τ_ϕ are the flux quantum, intralayer Fermi velocity, and phase coherence lifetime, respectively], the susceptibility $\chi_{\alpha\beta}$ is diagonal in the *crystal* representation, resulting in an ordinary (anisotropic mass) θ dependence at fixed T near T_c. At very high fields in very high-quality single crystals ($\omega_c\tau_\phi\gg1$, where ω_c is the pair cyclotron frequency), $\mathbf{M}$ is best evaluated in the *field* representation. The component $M_{\mathbf{B}}(\theta,T)$ exhibits anomalous oscillations in its θ dependence, arising from degenerate multiple minima in the pair potential, provided that the effective high-momentum cutoff q_c^* is sufficiently large. In this field regime, q_c^* is either on the order of $\pi s/a$, where a is the intralayer oxygen site repeat distance, or equal to $\pi[1+(B/B_0)\sin\theta]$. The oscillations are similar to de Haas–van Alphen oscillations in the B dependence of the normal state $\mathbf{M}$. They are broadened by local, clean-limit dynamic effects but should be observable for $\tau_\phi k_B T_c/\hbar\gg1$ and $N\geq2$, which we argue is the case in the best samples. In addition, the fluctuation specific heat (FSH) and Aslamazov-Larkin conductivity are calculated for $\mathbf{B}=0$, including dynamic effects. For arbitrary N, the FSH above T_c is found to be proportional to $\chi_{cc}(T)/T$. For fits of the theoretical FSH to experimental data, it is necessary to modify the mean-field expressions for $T<T_c$, such that the entropy of the superconducting transition remains zero. An example of such a modification is given. All fluctuation quantities exhibit dimensional crossover (DCR) from 3D behavior near T_c to 2D behavior further from T_c. For the fluctuation diamagnetism the DCR temperature $T_0(\theta)$ depends strongly upon θ in the vicinity of $\pi/2$, where it diverges. Away from T_c dynamic effects are found to be important and can be so strong as to mimic DCR behavior, even for $\theta=\pi/2$, for which DCR should not occur. The dynamic effects make quantitative corrections to the fluctuation quantities for T as close as 1 K to T_c. For $N=2$ detailed plots of the above fluctuation quantities for a range of the microscopic parameters are presented.

I. INTRODUCTION

Since there is to date no consensus on the microscopic mechanism for the copper oxide superconductors, a phenomenological model capable of making predictions for the superconducting properties of the entire class of materials may prove useful. There has recently been some evidence accumulating as to the symmetry of the order parameter (OP) in $YBa_2Cu_3O_{7-\delta}$ (Y 1:2:3). Muon-spin-relaxation experiments[1] and mixed-state-magnetization measurements[2] have indicated no deviation from the BCS-like temperature (T) dependence of the penetration depth λ with applied magnetic field $\mathbf{H}$ direction. ^{17}O NMR results[3] have shown some evidence of a Hebel-Schlichter peak just below the transition temperature T_c, although contradictory results have very recently become available.[4] Far-infrared measurements[5] gave a good fit to the Mattis-Bardeen (BCS) formula. More recent measurements[6] are qualitatively consistent with the BCS clean-limit result.[7] Recent high-resolution x-ray-diffraction measurements[8] have not seen any evidence for a coupling of the orthorhombic strain of the OP. Together, these experiments strongly suggest a nodeless OP in momentum space.

The mobile quasiholes (arising from the holes in excess of one per Cu site) are essentially restricted to being on the oxygen sublattice within the CuO_2 planes and on the bridging oxygen sites adjacent to the CuO_2 planes, except during interlayer tunnelling, as evidenced in $La_{2-x}Sr_xCuO_4$ by electron-energy-loss spectroscopy[9] and neutron scattering[10] experiments. The Cu^{2+} holes are localized[10] for $x=0$, with a Mott-Hubbard gap, and exhibit spin fluctuations.[11] These Cu^{2+} holes play some role in the superconductivity, however, as evidenced by NMR experiments.[3,4] For materials such as Y 1:2:3 (for $\delta<0.4$) which are superconducting, recent angular-resolved-photoemission experiments[12] have demonstrated the existence of a clear Fermi edge, proving that the normal state above T_c is a Fermi liquid. The normal-state

resistivity ρ_{ij} is extremely anisotropic, as demonstrated in a Bi compound by Martin *et al.*[13] In addition to a much larger magnitude, the ρ_{cc} has a different T dependence from ρ_{aa} or ρ_{bb}, as was found[14] in TaS_2(pyridine)$_{1/2}$. This demonstrates convincingly that the interstitial layers between the conducting planes are insulating.

Within the last two years, there have been several reports[15–17] of observations of superconducting fluctuations in the copper oxide materials. These fluctuations have been reported in the conductivity,[15] the specific heat,[16] and the magnetization.[17] In measurements of $\rho_{ij}(T)$, the downturn from quasilinear behavior in ρ_{aa} and ρ_{bb} has been attributed[15] to fluctuations, appearing to exhibit dimensional crossover (DCR) from three-dimensional (3D) behavior near to T_c to 2D behavior further from T_c. This attribution was based upon a fit to the Lawrence-Doniach[18] (LD) static result for the (s wave) Gaussian fluctuation conductivity in a layered superconductor. In that model, one layer per unit cell edge is assumed.

In the specific-heat report,[16] an analysis based upon the 3D Gaussian regions both above and below T_c led the authors to conclude that the ratio of the fluctuation specific heat (FSH) above T_c to that below T_c was too large to be consistent with s-wave OP symmetry. However, as we shall see in the following, those authors did not perform a self-consistent fit, as they did not account for the substantial entropy of the FSH. Very recently, however, those authors[16] have performed measurements upon a very high quality single crystal, and have concluded that the best fit to their new data is for an s-wave superconductor. In the conductivity[15] and specific-heat[16] data, and also in recent dc magnetization measurements[19] of the upper critical field H_{c2}, the coherence lengths extracted were sufficiently short as to limit the electrodynamics to the local limit, except in very large fields.

In the magnetization measurements,[17] precursor superconducting fluctuation diamagnetism (SFD) was reported, but no attempt to fit the data with available theory was made. This is not too surprising, as the available theory[18,20,21] to date is only for the case $\mathbf{H}\|\hat{\mathbf{c}}$, and the experiments were performed on powder samples. Hence we believe it would be useful to perform calculations of all three of these fluctuation quantities, accurate enough to perform fits over the majority of the T range of the observations, and specific to the copper oxide materials. We recall that fluctuations above T_c are expected to be observable for $T_c < T \lesssim 2T_c$, as was found in Pb/Tl alloys.[22]

In this paper, we present a model that we believe should prove useful in fits to the superconducting fluctuation and other behavior of the copper oxide superconductors. The model is a straightforward generalization of the LD model[18] for s-wave layered superconductors, generalized to include N conducting (CuO_2, presumably) layers within a c-axis repeat distance (unit cell edge) s, with $N-1$ equal spacings d, and Josephson tunneling parameters ζ_1 and ζ_2 between the different spacings d and d'; $s=(N-1)d+d'$. For those materials such as Y 1:2:3 exhibiting Cu-O chains, we assume that the chains are essentially inert, as the pairing of quasiholes is assumed to take place in the conducting layers (either the CuO_2 or bridging oxygen layers), not in the chains. The presence of the chains could cause an anisotropy of the pair effective mass within the nearby layers, which we include whenever possible. To our knowledge, this model encompasses all of the Cu-O superconductors known to date.

We solve this model explicitly for the Gaussian fluctuation free energy for $N \leq 4$. For $\zeta_1 \neq \zeta_2$, only one of the OP's found to have the "bare" T_c value (unreduced from its $\zeta_1=\zeta_2=0$ mean-field value), the others having lower T_c values. Near to T_c, the 3D fluctuations are dominated by this single OP. For ζ_1 comparable to ζ_2, additional OP's make substantial (but unequal) contributions to the 2D regime, their relative contributions depending upon ζ_1 and ζ_2. For arbitrary N, we calculate the angular (θ) and T dependence of the SFD, $\mathbf{M}(\theta,T)$ for both weak and strong fields. For quantitative comparison of the theory with experiment, we have generalized our model to the level of the time-dependent Ginzburg-Landau model, including the dynamic effects present in the local, clean limit. In order to determine the material parameters as consistently as possible, we have also performed the analogous calculations for the zero-field FSH above and below T_c, and for the (free energy-derivable) zero-field fluctuation conductivity. For comparison with experiment, we have presented detailed plots of these quantities for a range of microscopic parameters for $N=2$.

The outline of the paper is as follows: In Sec. II, we present the model, and solve for the eigenvalues of the Hamiltonian. In Sec. III, we calculate the SFD in the static limit. We consider both the weak field regime (Sec. III A), for which the quantization axes are those of the crystal, and the strong-field regime (Sec. III B), for which the field itself defines the quantization axis. In Sec. IV, we extend our results for the SFD to include dynamic effects. In Sec. V, the FSH is calculated. The fluctuation conductivity tensor is calculated at the same (above) level of approximation in Sec. VI. Finally, in Sec. VII, we present a summary and discussion of our results.

II. THE MODEL

We propose that the superconducting free energy is of the form

$$
\begin{aligned}
F_s - F_n = \sum_{j=1}^{M} \int_{js}^{(j+1)s} dz \int d^2\mathbf{r} \Bigg[& \sum_{n=1}^{N} \Bigg\{ a(T)|\psi_{jn}(\mathbf{r})|^2 + (b/2)|\psi_{jn}(\mathbf{r})|^4 + \sum_{\mu=1,2} (2m_\mu)^{-1} |(i\partial_\mu - 2eA_\mu)\psi_{jn}|^2 \Bigg\} \\
& + \zeta_1 \sum_{n=1}^{N-1} \left| \psi_{jn} \exp\left[-2ie \int_{js+(n-1)d}^{js+nd} A_3 dz \right] - \psi_{j,n+1} \right|^2 \\
& + \zeta_2 \left| \psi_{jN} \exp\left[-2ie \int_{js+(N-1)d}^{(j+1)s} A_3 dz \right] - \psi_{j+1,1} \right|^2 + \mathbf{B}^2/(8\pi) \Bigg] ,
\end{aligned}
\tag{1}
$$

where M is the number of unit-cell edges, $\psi_{jn}(\mathbf{r})$ is the (s wave) complex OP at the position $\mathbf{r}$ on the nth layer in the jth unit cell edge, m_μ is the intralayer effective mass in the $\hat{\mathbf{a}}$ ($\mu=1$) and $\hat{\mathbf{b}}$ ($\mu=2$) directions, $a(T)=a_0(T-T_c)$ (near to T_c) and b are the usual GL parameters, ζ_1 and ζ_2 are respectively the weak intracell and intercell interlayer couplings due to Josephson-like tunneling of quasihole pairs with charge $+2|e|$, A_μ and A_3 are the magnetic vector potential components, $\mathbf{B}=\nabla\times\mathbf{A}$, $\partial_\mu\equiv\partial/\partial x_\mu$, $s=d(N-1)+d'$, and we have set $c=\hbar=1$. In these units, the flux quantum $\phi_0=\pi/|e|$. All parameters (other than ψ_{jn}) are assumed independent of layer index, for simplicity. Equation (1) reduces to the form of Klemm, Luther, and Beasley[23] (KLB) for $N=1$, which is an extension of the LD model[18] to an arbitrary local magnetic field $\mathbf{B}$ direction. The phase factors in the tunneling terms are necessary to insure gauge invariance of the free energy. Nonlocal effects are neglected.

Very recently, there have been reports[24] of copper oxide superconductors doped with *electrons* rather than holes. This phenomenological model can easily treat those materials as well, with a change in the sign of the quasiparticle pair charge to $-2|e|$.

In the Gaussian regime above T_c, the $|\psi|^4$ term can be neglected. In this regime, $\mathbf{B}$ is constant both in direction and in magnitude, and essentially equal to $\mathbf{H}$, differing from $\mathbf{H}$ only by the (small) fluctuation magnetization. We take $\mathbf{B}=B(\sin\theta\cos\phi,\ \sin\theta\sin\phi,\ \cos\theta)$ with respect to $\hat{\mathbf{a}}$, $\hat{\mathbf{b}}$, and $\hat{\mathbf{c}}$. The resulting Gaussian fluctuation free energy is minimized with respect to variations in ψ^*_{jn}, leading to an eigenvalue equation for each ψ_{jn}. We define $\varepsilon_1\equiv 2\zeta_1$, $\varepsilon_2\equiv\zeta_1+\zeta_2$, $\gamma_\nu\equiv-\zeta_\nu\exp(i\phi_\nu)$ for $\nu=1,2$, where $\phi_1=q_z d$, $\phi_2=q_z d'$, $q_z=k_z-2eA_3$, $q\equiv q_z s$, and k_z is the wave vector in the $\hat{\mathbf{c}}$ direction,

$$\psi_{jn}=(Ms)^{-1/2}\sum_{|k_z|\le\pi/s}\psi_{k_z n}\exp\{ik_z[js+(n-1)d]\}\ .$$

Defining $H_0=K+V_0$ to be the intralayer part of the Hamiltonian, the full Hamiltonian $H=K+V$ differs from H_0 by purely interlayer potential-energy-like terms. In essence, the pairs on a given layer move with kinetic energy K, feel the (harmonic) potential V_0 due to their direct interaction with the magnetic field, but also feel the field-dependent potentials $(V-V_0)$ due to the presence of the other layers.

If the crystal were not periodic, we would have to diagonalize an $NM\times NM$ matrix, containing nonvanishing elements along the diagonal and the positions neighboring the diagonal. In this case, the periodicity of the lattice forces the amplitudes of ψ_{jn} and $\psi_{j'n}$ to be equal, so it is possible to sum up all of the contributions to $V-V_0$ by diagonalizing an $N\times N$ matrix. For general N, the problem maps onto that for the calculation of the phonon bands for N atoms in a one-dimensional unit cell.[25] Since

$$[H-H_0,V]=[H-H_0,V_0]=0\ ,$$

we let $\bar{\lambda}$ be any eigenvalue of $H-H_0$. This diagonalization is exact for $\mathbf{B}\|\hat{\mathbf{c}}$. For a complete treatment for an arbitrary direction of $\mathbf{B}$, see the Appendix.

For $N=2$, we must diagonalize a 2×2 matrix, which is easily done by solving the determinant equation

$$\begin{vmatrix}\varepsilon_2-\bar{\lambda} & \gamma_1^*+\gamma_2\\ \gamma_1+\gamma_2^* & \varepsilon_2-\bar{\lambda}\end{vmatrix}=0\ , \tag{2}$$

for which the eigenvalues are

$$\bar{\lambda}_\pm=\zeta_1+\zeta_2\pm[\zeta_1^2+\zeta_2^2+2\zeta_1\zeta_2\cos(q)]^{1/2}\ . \tag{3}$$

The eigenvectors for $N=2$ are

$$\tilde{\psi}_{k_z\pm}=\exp(i\eta_1)[\psi_{k_z1}\pm\exp(i\eta_2)\psi_{k_z2}]/\sqrt{2}\ ,$$

respectively, where η_1 and η_2 depend upon ϕ_1 and ϕ_2. Note that for $\zeta_1=\zeta_2=\zeta$ and $s=2d$, $\bar{\lambda}_-$ reduces to the LD form, $2\zeta[1-\cos(q_z d)]$. For either $\zeta_1\ll\zeta_2$ or $\zeta_2\ll\zeta_1$, $\bar{\lambda}_-$ is again of the LD form, $J[1-\cos(q)]$, where $J=\zeta_1\zeta_2/(\zeta_1+\zeta_2)$. In addition, there is the $\bar{\lambda}_+$ band, of energy $2(\zeta_1+\zeta_2)-J\cos(q)$. For the special case that $\zeta_1=\zeta_2$, we have

$$\bar{\lambda}_\pm=2\zeta[1\pm\cos(q/2)]\ .$$

This case is pictured in Fig. 1(a). For this special case, the bands are degenerate at $q=\pi$. More generally, for $\zeta_1\neq\zeta_2$, this degeneracy is removed, as pictured in Figs. 1(b) and 1(c). Since the 3D regime of the fluctuations arising from the low-energy band (with the highest-T_c value) is for $a(T)$ less than the maximum in this band, the higher-energy band will make at best a weak relative contribution to the 3D fluctuation regime, unless ζ_1 and ζ_2 are nearly equal. It can make a substantial relative contribution to the 2D fluctuation regime above T_c, provided that ζ_1 and ζ_2 do not differ greatly in magnitude.

The new physics comes from the existence of the second eigenvalue $\bar{\lambda}_+$, analogous to an optical phonon band. In ordinary superconductors, one would have such additional order parameter bands, but the intersite hopping energies would be much larger (i.e., on the order of 1–5 eV) than in the copper oxides, making those bands unobservable in the fluctuations. The relevant parameter here is ζ_1, for which there is no direct measure to date. However, one would expect[23] $\zeta_1\sim|J_1|^2/4\pi T_c$, $\zeta_2\sim|J_2|^2/4\pi T_c$, for small $|J_i|/4\pi T_c$, where J_1 and J_2 are the single quasihole tunneling energies in the normal state.

Positron annihilation studies[26] in Y-Ba-Cu-O have shown a doubly periodic quasihole Fermi surface with flat regions in the $\hat{\mathbf{c}}^*$ axis direction in reciprocal space, the amplitudes of the two components being comparable to each other. We thus expect $J_1\lesssim 2J_2$, so that $\zeta_1\lesssim 4\zeta_2$ for that material. Since the DCR temperature T_0 in that material has been claimed from conductivity measurements[15] to be roughly 15 K above T_c, this would imply $\zeta_2\lesssim 30$ K. In the copper oxides, some of the Bi and Tl compounds are extremely anisotropic, presumably due to the very small ζ_2 values, as one might expect the ζ_1 values for these materials to be roughly the same as in Y-Ba-Cu-O. However, the $N=3$ compounds, for example, have a different CuO_2 layer sandwiched between two

other layers, the middle layer not having any bridging oxygens out of the plane, unlike the other two layers. Hence, it is entirely possible that in materials containing layers without bridging oxygens, the ζ_1 values for Josephson tunneling between these layers and the neighboring CuO_2 layers could be significantly different than in those materials containing only layers with bridging oxygens. For example, the Tl or Bi layers might either facilitate the tunneling in the ζ_2 process, or be conducting. There is also the possibility that the "layers" of bridging oxygens might be the primary conducting layers. In that case, the effective N would be just 2, even for 3 or more CuO_2 layers per unit cell edge.

We note further that this is a phenomenological model, in which the effects of intrinsic Josephson tunneling as well as extrinsic effects (e.g., electrical shorts due to crystal imperfections) are taken into account in those parameters. Such shorts might tend to make ζ_1 and ζ_2 closer to each other in magnitude, increasing both of their values. Thus, for a variety of reasons, values for ζ_1 could be at least comparable to ζ_2 in some materials, causing the higher-energy bands to contribute significantly to the observed fluctuations above T_c, especially in the 2D regime.

For $N=3(4)$, one must diagonalize a 3×3 (4×4) matrix, leading to

$$\begin{vmatrix} \varepsilon_2-\bar{\lambda} & \gamma_1^* & \gamma_2 \\ \gamma_1 & \varepsilon_1-\bar{\lambda} & \gamma_1^* \\ \gamma_2^* & \gamma_1 & \varepsilon_2-\bar{\lambda} \end{vmatrix}=0 \tag{4a}$$

and

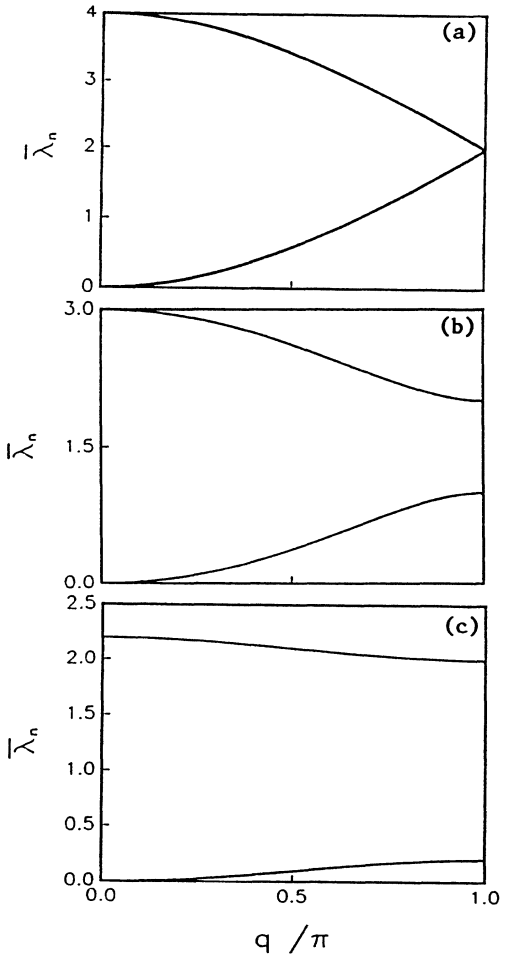

FIG. 1. Shown are the energy bands for $N=2$. The energy scale is set by defining $\max(\zeta_1,\zeta_2)=1$, in arbitrary units. (a) $\zeta_1=\zeta_2$; (b) $\zeta_2=\frac{1}{2}\zeta_1$; (c) $\zeta_2=\zeta_1/10$.

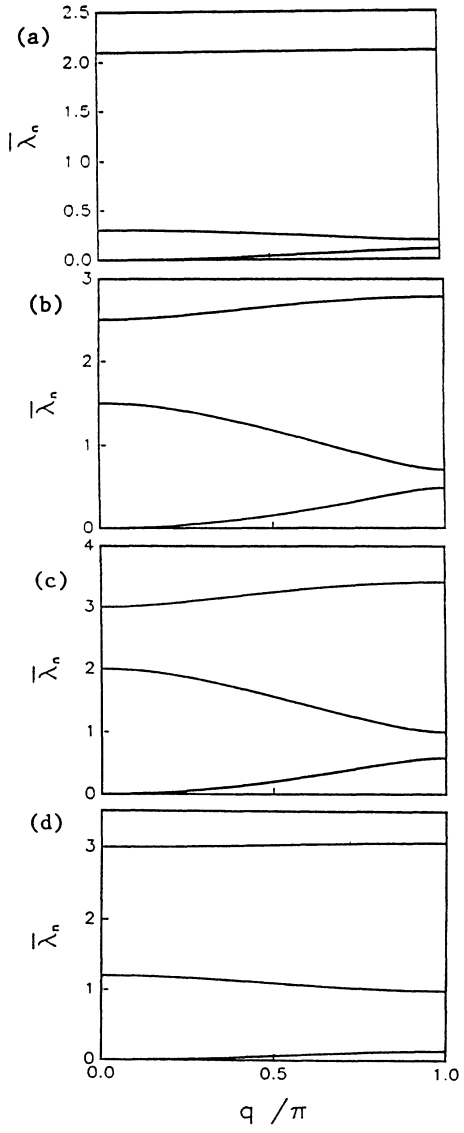

FIG. 2. Shown are the energy bands for $N=3$. The energy scale is set by defining $\max(\zeta_1,\zeta_2)=1$, in arbitrary units. (a) $\zeta_1=\zeta_2/10$; (b) $\zeta_1=\zeta_2/2$; (c) $\zeta_2=\zeta_1/2$; (d) $\zeta_2=\zeta_1/10$.

$$\begin{vmatrix} \varepsilon_2-\bar{\lambda} & \gamma_1^* & 0 & \gamma_2 \\ \gamma_1 & \varepsilon_1-\bar{\lambda} & \gamma_1^* & 0 \\ 0 & \gamma_1 & \varepsilon_1-\bar{\lambda} & \gamma_1^* \\ \gamma_2^* & 0 & \gamma_1 & \varepsilon_2-\bar{\lambda} \end{vmatrix} = 0 , \tag{4b}$$

resulting in a cubic (quartic) equation for the eigenvalues,

$$\bar{\lambda}^3-2(2\zeta_1+\zeta_2)\bar{\lambda}^2+3\zeta_1(\zeta_1+2\zeta_2)\bar{\lambda}=2\zeta_1^2\zeta_2[1-\cos(q)] , \tag{5a}$$

and

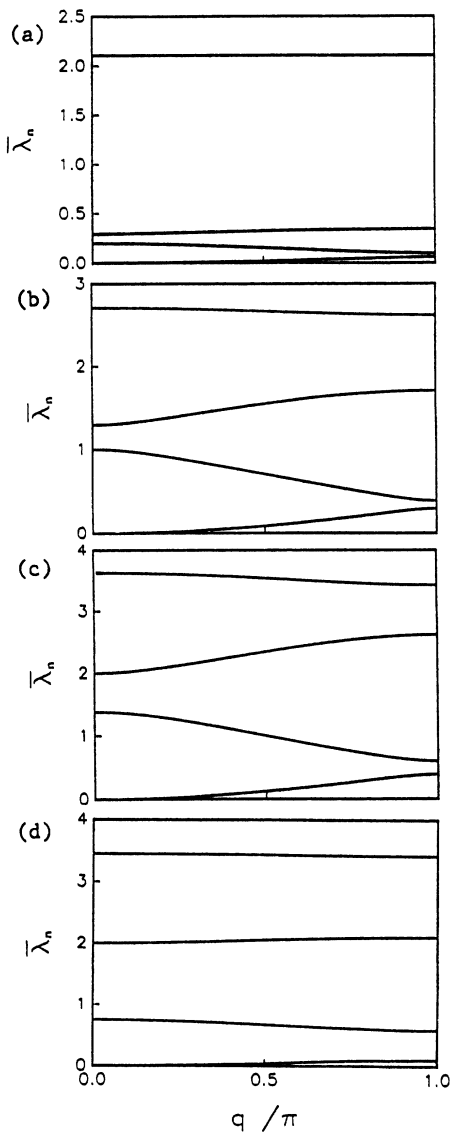

FIG. 3. Shown are the energy bands for $N=4$. The energy scale is set by defining $\max(\zeta_1,\zeta_2)=1$, in arbitrary units. (a) $\zeta_1=\zeta_2/10$; (b) $\zeta_1=\zeta_2/2$; (c) $\zeta_2=\zeta_1/2$; (d) $\zeta_2=\zeta_1/10$.

$$\bar{\lambda}^4-2(3\zeta_1+\zeta_2)\bar{\lambda}^3+5\zeta_1(2\zeta_1+2\zeta_2)\bar{\lambda}^2-4\zeta_1^2(\zeta_1+3\zeta_2)\bar{\lambda} = -2\zeta_1^3\zeta_2[1-\cos(q)] , \tag{5b}$$

for $N=3(4)$, respectively. In the Ginzburg-Landau (3d) regime, the effective mass m_{30} in the $\hat{c}$ direction for the lowest-energy band is obtained by expanding $\cos(q)$ to order q^2, and solving for the lowest eigenvalue. This eigenvalue has a T_c value that is not suppressed by the interlayer tunneling energies. It is readily apparent that for arbitrary N,

$$m_{30}=N[(N-1)/\zeta_1+1/\zeta_2]/(2s^2) , \tag{6}$$

analogous to the overall resistance (in appropriate units) of $N-1$ resistors of value $1/(2s^2\zeta_1)$ in series with one of value $1/(2s^2\zeta_2)$. Note that for $N=1$, $m_{30}=1/(2\zeta_2 d'^2)$, and as $N\to\infty$, $m_{30}\to 1/(2\zeta_1 d^2)$, as expected. Equation (6) has been explicitly checked for $N\le 6$.

For $\zeta_1=\zeta_2=\zeta$ and N arbitrary, the bands may be readily calculated, yielding

$$\bar{\lambda}_{n'}=2\zeta\{1-\cos[(q+2n'\pi)/N]\} \quad \text{for } n'=0,1,\ldots,N-1 , \tag{7}$$

respectively. Henceforth, we shall relabel the band index subscript n to rank order the bands in increasing energy: $\bar{\lambda}_0<\bar{\lambda}_1<\bar{\lambda}_2<\cdots$. The special case described by Eq. (7) arises from a single (noninteracting) tight-binding band of overall width 4ζ that has been folded back and forth at $q=0$ and at the zone boundary $q=\pi$, as pictured in Fig. 1(a) for $N=2$. For $\zeta_1\neq\zeta_2$, the degeneracies of the bands at $q=0$ and π are lifted, as is shown for $N=3$ and 4 in Figs. 2 and 3. The T_c values for each of the bands is given by

$$a(T_{cn})=\min_q(\bar{\lambda}_n) , \tag{8}$$

so that only the lowest ($n=0$) band has no suppression in T_c due to the interlayer couplings. The DCR temperature T_{0n} for the nth OP band in zero field is

$$a(T_{0n})=\max_q(\bar{\lambda}_n) . \tag{9}$$

For the (unlikely) case $\zeta_1\ll\zeta_2$, at least one (and sometimes several) OP's other than that corresponding to the ground state will contribute significantly to the 2D fluctuation regime. When $\zeta_2<\zeta_1$, the higher bands are only important (even in the 2D regime) for ζ_1 and ζ_2 of the same order of magnitude. For $\zeta_2\ll\zeta_1$, the top of the $n=0$ band is well below the bottom of the next lowest band ($n=1$), so the fluctuations above T_c are well approximated by neglecting the higher bands altogether. In no case do the bands overlap, so that these additional OP bands will only make a small numerical correction to the 3D fluctuation regime (relative to the divergent behavior near to T_c for the $n=0$ band), unless ζ_1 and ζ_2 are nearly equal.

III. FLUCTUATION DIAMAGNETISM

To illustrate the above, we have first calculated the SFD in this model. Since the experiments until very recently were performed on powder samples, it is necessary

to calculate the SFD at an arbitrary direction of **B**, and then to do a powder average over all of the crystallites in the sample. However, as measurements on an aligned powder have just become available,[27] we have kept the full angular dependence of the fluctuation magnetization **M**. We consider the weak and strong-field regimes separately. These regimes are given by $\omega_c\tau_\phi \ll 1$ and $\omega_c\tau_\phi \gg 1$, where

$$\omega_c = 2eB/(m_i m_j c^2)^{1/2}$$

is the pair cyclotron resonance frequency for **B** normal to the $x_i x_j$ plane, and τ_ϕ is the effective (pair breaking) phase coherence lifetime arising from inhomogeneities. Note that the m_i are pair effective masses. As we shall see in the following, the weak-field regime is further restricted by

$$B < B_0 = \phi_0/(s v_F \tau_\phi) ,$$

where v_F is the Fermi velocity in the ab plane.

In the weak-field regime ($\omega_c\tau_\phi \ll 1$), the pairs complete at most a small fraction of a Landau orbit before dissociating, so that the notion of a Landau orbit is essentially meaningless. In this limit, it is most natural to choose the quantization axes to be those of the crystal, just as in a correct calculation of Landau diamagnetism in a crystal. However, the susceptibility $\chi_{\alpha\beta}$ is only diagonal in this representation (even in the $B \to 0$ limit) for a finite phase coherence length $L_\phi = v_F\tau_\phi$, due to complications in taking the thermodynamic limit, arising from degeneracy effects. We note that in addition to the sum over the discrete "Landau" orbits, one must integrate over the continuous degrees of freedom k_α in calculating $\chi_{\alpha\alpha}$.

In the strong-field regime ($\omega_c\tau_\phi \gg 1$), the pairs complete many Landau orbits, so that **M** is best evaluated in the representation defined by the magnetic field direction, as in the case of the de Haas-van Alphen (dHvA) effect. In this limit **M** contains the components $M_{\mathbf{B}}$, M_θ, and M_ϕ, respectively, where $\hat{\theta}$ and $\hat{\phi}$ are unit vectors normal to **B**. Practically speaking, as long as the pairs complete at least a substantial fraction of an orbit ($\omega_c\tau_\phi \gtrsim 0.1$), the field representation will be sensible. We note that one could attempt to solve for the strong-field regime in the crystal axis representation, expanding the nonlinear elements of M_α in powers of $\{B_\alpha\}$. However, as in the case of the dHvA effect, one would require a large number (>10) of powers in the $\{B_i\}$ to obtain a convergent expansion (unless the pair bands were nearly ellipsoidal in symmetry), as periodic functions are not well approximated for arbitrary argument values by a finite power series. More important, *one must take a proper account of the degeneracies of the eigenvalues.* Such an expansion would thus necessarily be limited to weak field regime.

We first consider the case $\mathbf{B}\|\hat{\mathbf{c}}$. Choosing **A** to depend solely upon y results in a degeneracy with respect to k_x values that can be removed by a shift in y, giving rise to the Landau degeneracy factor. One must integrate over the continuous variable k_z, which appears in $\bar{\lambda}_n(sk_z)$. For $\mathbf{B}\|\hat{\mathbf{c}}$, there is only one minimum in the (harmonic) potential; the discrete eigenvalues are nondegenerate.

The case of $\mathbf{B}\|\hat{\mathbf{a}}$ (or $\hat{\mathbf{b}}$) is very different. Consider the simplest case of the LD pair band,[23]

$$\bar{\lambda} = J[1-\cos(k_z s + 2eBsy)] ,$$

setting $\tau_\phi = \infty$. In this case, the eigenvalue equation is the Mathieu equation in the dependent (position) variable y. Even for a finite crystal, the $k_z s$ in the argument of $\bar{\lambda}$ can be eliminated by a shift in y (which amounts to adding a constant to A_3), giving rise to the Landau degeneracy factor. One must integrate over the (unbounded) continuous degrees of freedom k_x, which appears in the free-particle form $k_x^2/2m_1$. For an infinite crystal, $\bar{\lambda}$ has an infinite number of degenerate absolute minima, leading to bands of eigenvalues for $B \neq 0$, and infinitely degenerate discrete harmonic oscillator levels for $B = 0$. A good picture of this is given by McLachlan.[28] This is analogous to the tight-binding principle for the energy levels of a periodic array of N atoms a variable distance apart.

For $\mathbf{B}\|\hat{\mathbf{a}}$ and finite effective length L in the $\hat{\mathbf{b}}$ direction, the degeneracy of the eigenvalues depends upon L. If $B < B_0 \equiv \phi_0/(sL)$, there can be only one absolute minimum of the potential, and the corresponding low-energy eigenvalues are nondegenerate. For $B > 3B_0/2$, there are at least two degenerate absolute minima. For $s = 12$ Å and $L = 10$ μm, the eigenvalues are nondegenerate for $B_0 = 1.7$ kG, so this limit ($B < B_0$) is very relevant in large ($L > 10\,\mu$m), untwinned single crystals. In samples with grain size L_g or intertwin distance L_t, $L \gtrsim \min(L_g, L_t)$. This is because the OP's on opposite sides of a twin or in different grains are weakly coupled, differing in phase. In Ya-Ba-Cu-O, $L_t \ll L_g$ (except for isolated parts of the best single crystals), empirically[29] obeying $L_t \simeq C(L_g)^{1/2}$ for $2 \le L_g \le 50$ μm, where $C \simeq 1.7$ (Å)$^{1/2}$. For $L_t = 10^3$ Å, $B_0 = 17$ T. We therefore interpret the effective length L as the phase coherence length $L_\phi = v_F\tau_\phi$ in the ab plane.

For a tensor representation for the SFD to be valid, one must be able to calculate all tensor elements in that representation. Hence, even for $B \to 0$, the crystal representation is only useful for a finite L_ϕ. $\chi_{\alpha\beta}$ is only diagonal in this representation for the fully nondegenerate case $B < B_0$. If degeneracies in the absolute potential minimum are allowed, χ_{ij} develops nonanalytic off-diagonal terms. For example, terms such as $(B_x)^{3/2}(B_z)^{1/2}$ in the free energy, while proportional to B^2, cannot be properly treated in the crystal representation.

For an isotropic pair excitation spectrum, the SFD was calculated using the field quantization procedure by Schmid.[30] For an ellipsoidal pair excitation spectrum (analogous to an ellipsoidal Fermi surface in ordinary Landau diamagnetism), both field and crystal quantization procedures give the same result for all field strengths, due to the rotational invariance of the pair excitation spectrum (in appropriately scale-transformed coordinates). For a general pair excitation spectrum, as for a general Fermi surface, these procedures give demonstrably identical results for fields along one of the crystal axes. For arbitrary field angles, they should also give identical results. For the technical reasons already

noted, however, one has to be very careful in taking the thermodynamic limit. The calculations are nontrivial except for the two cases we shall consider: The weak-field limit ($\omega_c\tau_\phi \ll 1$) with no degeneracies ($B < B_0$) in the crystal representation, and the strong-field case ($\omega_c\tau_\phi \gg 1$) in the field representation, introducing a high-momentum cutoff to avoid such thermodynamic limit problems.

We shall argue in the following that for the best superconducting copper oxide samples, both field regimes are experimentally accessible. Our exact expressions can readily be evaluated numerically, even in the presence of local, clean-limit dynamics.

A. Weak fields

In weak fields such that $\omega_c\tau_\phi \ll 1$ and $B < B_0$, we use the crystal representation, $\mathbf{B}=(B_x,B_y,B_z)$, and the SFD volume susceptibility

$$\chi_{\alpha\beta}(T) = -\partial^2(F/V)/\partial B_\alpha \partial B_\beta \ ,$$

where F is the Helmholtz free energy. It is easy to show that $\chi_{\alpha\beta}$ is diagonal ($\chi_{\alpha\beta}=\chi_{\alpha\alpha}\delta_{\alpha\beta}$) for any choice of $\mathbf{A}$. We therefore consider only the cases of $\mathbf{B}$ parallel to one of the crystal axes ($\hat{\mathbf{x}}_\alpha$) expand F to order B_α^2 to calculate the zero-field $\chi_{\alpha\alpha}$, and then take the thermodynamic limit, guaranteeing that $BL_\phi \to 0$.

For $\mathbf{B}\|\hat{\mathbf{x}}_\alpha$, the Gaussian partition function Z may be written after the OP diagonalization as

$$Z = \left[\prod_{k_\alpha,n,p,g} \int D^2\tilde{\psi}_{k_\alpha np}\right] \exp[-\beta(F_S - F_N)] \ , \quad (10)$$

where

$$F_S - F_N = \sum_{g=1}^{N_\phi} \sum_{n=0}^{N-1} \sum_{p=0}^{\infty} \sum_{k_\alpha} \tilde{E}_{k_\alpha np} |\tilde{\psi}_{k_\alpha np}|^2 \ , \quad (11)$$

the index p counts the Landau levels, k_α is the wave vector in the $\hat{\mathbf{x}}_\alpha$ direction ($\|\mathbf{B}$), N_ϕ is the number of flux quanta in the sample (i.e., the Landau degeneracy), and $\tilde{E}_{k_\alpha np}$ are the eigenvalues of the Hamiltonian (see the Appendix),

$$H_n \tilde{\psi}_{k_\alpha np} = \tilde{E}_{k_\alpha np} \tilde{\psi}_{k_\alpha np} \ , \quad (12a)$$

where

$$H_n = a(T) + \sum_{\mu=1,2} (2m_\mu)^{-1}(i\partial_\mu - 2eA_\mu)^2 + \bar{\lambda}_n(q) + \delta\tilde{\lambda}_n(q) \ . \quad (12b)$$

For $\alpha=1,2$ the sum over k_α in Eq. (10) is unrestricted. For $\alpha=3$, the sum is restricted by $|k_3| \le \pi/s$. For $\mathbf{B}\|\hat{\mathbf{c}}$ ($\alpha=3$), we choose $\mathbf{A}=-B_z y\hat{\mathbf{x}}$, yielding a harmonic oscillator Hamiltonian, with a dispersion along $\hat{\mathbf{B}}$ given by $\bar{\lambda}_n(sk_z)$. For $\mathbf{B}\|\hat{\mathbf{a}}$, we choose $\mathbf{A}=B_x y\hat{\mathbf{z}}$.

In order to calculate the Helmholtz free energy $F=-\beta^{-1}\ln(Z)$ (where $\beta=1/k_BT$) to order B_α^2, we need only find the eigenvalue to order B_α, due to the Landau degeneracy factor. For $\mathbf{B}\|\hat{\mathbf{c}}$, the eigenvalues are always proportional to B_z. For $\mathbf{B}\|\hat{\mathbf{a}}$, we may set $k_z=0$ (π/s) for n even (odd) inside the argument of $\bar{\lambda}_n$, as the k_z dependence of q is contained in the Landau degeneracy factor. We may then expand $\bar{\lambda}_n(2eB_x ys)$ [$\bar{\lambda}_n(\pi+2eB_x ys)$, for n odd] to order B_x^2, obtaining a harmonic oscillator Hamiltonian with a free-particle dispersion ($k_x^2/2m_1$) along $\mathbf{B}$. Results for $\mathbf{B}\|\hat{\mathbf{b}}$ are obtained by interchanging m_1 and m_2. We find

$$\chi_{xx} = \sum_{n=0}^{N-1} \frac{-\pi k_B T}{6\phi_0^2(m_2 m_{3n})^{1/2}} \times \int_{-\infty}^{\infty} \frac{dk_x}{2\pi[a(T)+a(T_{cn})+(k_x^2/2m_1)]} \ , \quad (13a)$$

$$\chi_{yy} = (m_2/m_1)\chi_{xx} \ , \quad (13b)$$

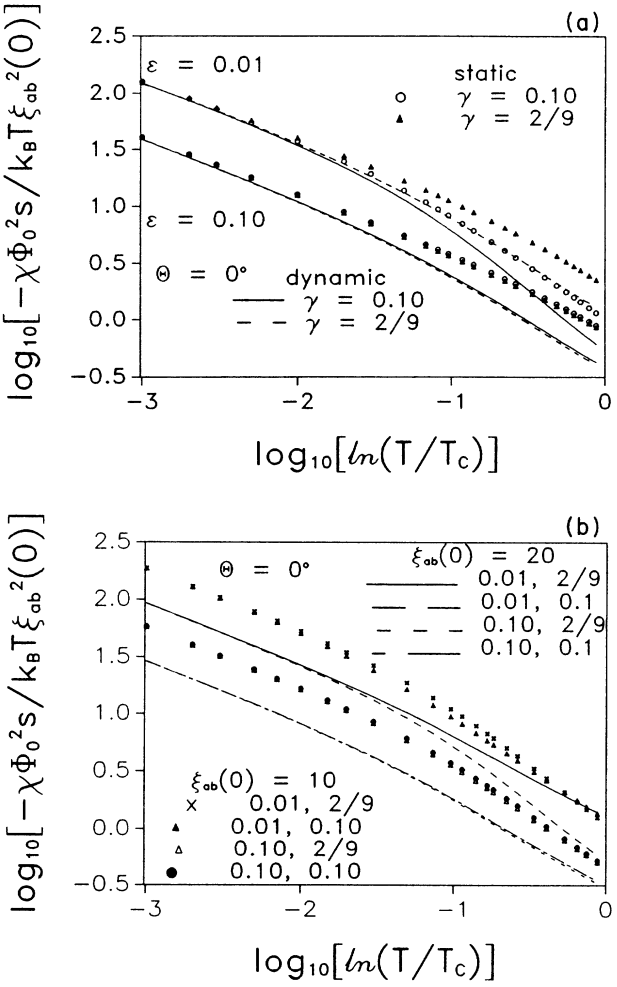

FIG. 4. Log-log plot of χ_{zz}/T versus $\ln(T/T_c)$ for $\theta=0°$ for both high and low fields. (a) $\xi_{ab0}(0)=15$ Å, $\varepsilon=0.1$ and 0.01, $\gamma=0.1$ and $\frac{2}{9}$. For $\varepsilon=0.01$, $\gamma=\frac{2}{9}$, both bands are included. The open circles and filled triangles are the results of the static approximation; solid and dashed lines are dynamic results for the same parameters. (b) $\xi_{ab0}(0)=20$ and 10 Å. The legend indicates ε and γ values. For $\xi_{ab0}(0)=10$ Å and $\varepsilon=0.01$, both γ values shown have $n=1$ contributions. All calculations are dynamic ones.

and

$$\chi_{zz}=\frac{-\pi k_B T}{6\phi_0^2(m_1 m_2)^{1/2}}\sum_{n=0}^{N-1}\int_{-\pi/s}^{\pi/s}\frac{dk_z}{2\pi[a(T)+\bar{\lambda}_n(sk_z)]}\ , \tag{13c}$$

where we have used Eq. (8) for the minimum in the OP band.

We remark that this simple form for the weak field $\chi_{\alpha\beta}$ leads to an angular dependence of the SFD that is of the anisotropic mass form,

$$\chi_{\rm eff}(\theta,\phi,T)=[\chi_{xx}\cos^2(\phi)+\chi_{yy}\sin^2(\phi)]\sin^2(\theta)+\chi_{zz}\cos^2(\theta)\ . \tag{13d}$$

We note that χ_{xx} (and χ_{yy}) has a 3D T dependence, containing two terms proportional, respectively, to $T/[\ln(T/T_{cn})]^{1/2}$, as the integral over k_x can be performed exactly. As discussed in the following, we have modified the form of $a(T)$ to coincide with that expected from BCS theory. This result shows clearly that there is no DCR in the T dependence of the SFD for $\mathbf{B}\perp\hat{\mathbf{c}}$. χ_{zz} depends differently upon T due to DCR effects, so that a simple T-independent anisotropic mass description of the SFD applies only in the 3D region for weak fields.

The powder average of $\chi_{\rm eff}(\theta,\phi,T)$ is easily found to be $\langle\chi\rangle=(\chi_{xx}+\chi_{yy}+\chi_{zz})/3$. In Figs. (4a) and (5a), we have presented plots of χ_{xx}/T and χ_{zz}/T for $\varepsilon(=m_1/m_{30})=0.1$ and 0.01, $\gamma[=\zeta_1\zeta_2/(\zeta_1+\zeta_2)^2]=0.1$ and 2/9, and $\xi_{ab0}(0)=15$ Å. Figures 4(b) and 5(b) are log-log plots of χ_{xx}/T and χ_{zz}/T for $\xi_{ab0}(0)=20$ Å and 10 Å, including the dynamic effects discussed in Sec. IV. Note that the static calculations of χ_{xx}/T plotted in Fig. 4(a) have slopes of $-\frac{1}{2}$.

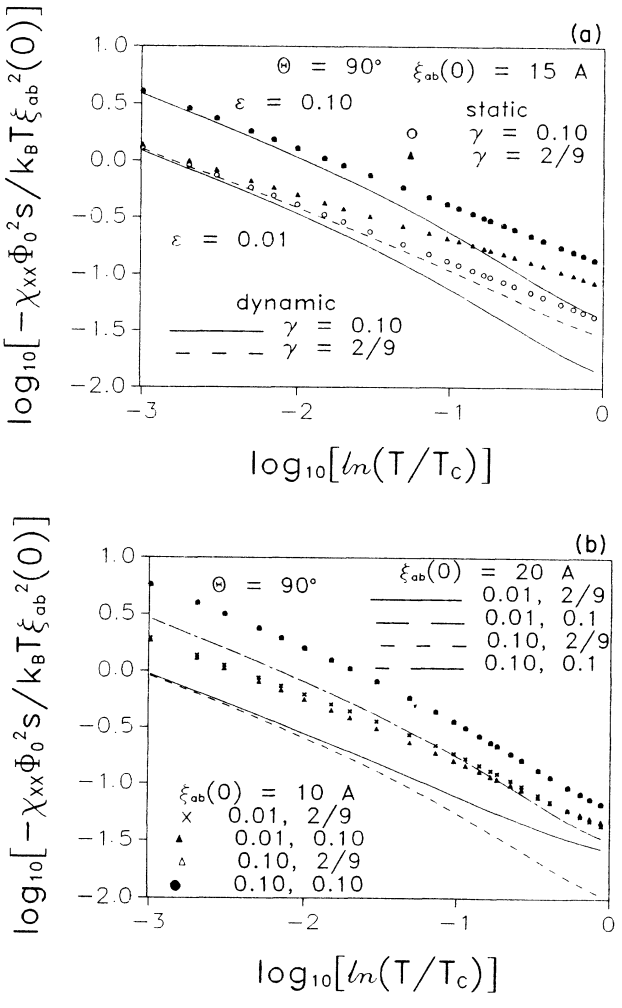

FIG. 5. Log-log plot of χ_{xx}/T vs $\ln(T/T_c)$ for $\theta=90°$ for low fields. (a) $\xi_{ab0}(0)=15$ Å, $\varepsilon=0.1$ and 0.01, $\gamma=0.1$ and $\frac{2}{9}$. For $\varepsilon=0.01$, $\gamma=\frac{2}{9}$, both bands are included. The open circles and solid triangles are the results of the static approximation; solid and dashed lines are dynamic results for the same parameters. (b) $\xi_{ab0}(0)=20$ and 10 Å. All calculations are dynamic ones.

B. Strong fields

We now turn to the more interesting case $\omega_c\tau_\phi\gg1$. This regime is attained when

$$B/\tilde{H}_{c2}(\theta)\gg\hbar/(\tau_\phi k_B T_c)\ ,$$

where

$$\tilde{H}_{c2}(\theta)\equiv T_c|\partial H_{c2}(\theta,T)/\partial T|\ ,$$

evaluated at T_c. If $\tau_\phi k_B T_c/\hbar$ were on the order of unity as has been suggested,[31] it would be impossible to study this high-field regime. From normal-state resistivities,[32] $\tau k_B T_c/\hbar\gtrsim1$, where τ is the single quasihole scattering time. However, we must have $\tau_\phi k_B T_c/\hbar\gg1$, since numerous workers have obtained essentially the same T_c values in each of the vast majority of the materials studied! If there were a shift of as much as 2 K down from the bare (homogeneous) T_{c0} (in the absence of pair-breaking effects), then the standard Abrikosov-Gor'kov pair-breaking theory would imply $\tau_\phi k_B T_c/\hbar\sim18$ in Ya-Ba-Cu-O. In the best samples, with the highest T_c values, we are very likely to have $\tau_\phi k_B T_c/\hbar\gtrsim100$ or larger.

The partition function in the Gaussian regime for strong fields is similar to that for weak fields, differing in one essential feature. Writing $\mathbf{B}$ in terms of its components in the crystal axis representation, as already noted, we must rotate the crystal axes so that one of them ($\hat{\mathbf{c}}$, for example) becomes parallel to $\mathbf{B}$, in order to quantize the Hamiltonian properly. In this limit, k_α in Eqs. (10) and (11) becomes replaced with $\tilde{k}_z$, the wave vector along $\mathbf{B}$. In addition, the summation over $\tilde{k}_z$ values is restricted to $|\tilde{k}_z|\le\tilde{k}_{z0}=\pi/s|\cos\theta|$, due to the rotation. This form for $\tilde{k}_{z0}$ is easily seen to be correct by considering an infinite thin slab of thickness $2\pi/s$ normal to $\hat{\mathbf{c}}^*$ in reciprocal space. As the integration is along the direction of $\mathbf{B}$, for $\theta=0$, $\tilde{k}_z=k_z$, which is bounded by $\pm\pi/s$. For $\theta=\pi/2$, $\tilde{k}_z=k_x$, which is unbounded, as already discussed. For $\mathbf{B}$ at an angle θ with respect to the normal to the slab, the integration limits are trivially found to be $\pm\pi/(s|\cos\theta|)$.

If τ_ϕ were infinite, we could use this procedure to calculate the weak-field regime (which would agree with

those of Sec. III A, provided that we first took $B \to 0$ before taking the thermodynamic limit): All (nondegenerate) potential minima would contain an infinite number of Landau levels, and the procedure would therefore be exact. By taking the thermodynamic limit before setting $B \to 0$ (the usual procedure), we are implicitly assuming an infinite degeneracy of the $B \to 0$ eigenvalues for $\theta = \pi/2$. As we shall see, these thermodynamic limit problems are easily handled in the field representation by introducing a cutoff q_c^* in the wave vector integration in the $\hat{\mathbf{c}}^*$ direction, which incorporates the $\tau_\phi < \infty$ restriction. However, $\tau_\phi < \infty$ also restricts the applicability of this approach to larger fields ($\omega_c \tau_\phi \gtrsim 1$).

In addition, the anharmonicities of the potential wells cause the eigenvalues to become nonlinear in B. However, we may approximate these potential wells by their exact minimum positions and curvatures, which is valid for $B/\tilde{H}_{c2}(\theta) \ll 1$. Hence, the region of (rigorous) validity of this strong-field calculation is

$$\hbar/(\tau_\phi k_B T_c) \ll B/\tilde{H}_{c2}(\theta) \ll 1 ,$$

which is theoretically attainable for $\tau_\phi k_B T_c/\hbar \gg 1$. As noted in the introduction to Sec. III, however, both procedures are exact for all field strengths for $\theta = 0$, neglecting nonlocal effects. However, for $B/\tilde{H}_{c2}(\theta) \ll 1$ and $\tau k_B T_c/\hbar \gtrsim 1$, nonlocal effects make at most a small correction to the local dynamic calculation results,[21,22,33] so our results should be accurate in this regime. Experimentally, the fields involved would most likely be in the range 10-50 T in untwinned ultra high-quality single crystals of Ya-Ba-Cu-O. In the Bi and Tl compounds, twinning is not a problem, so one "merely" needs homogeneous single crystals with a very sharp T_c.

For simplicity of the argument, we assume **B** lies in the ac plane, ($\phi = 0$). Results for $\phi = \pi/2$ can easily be found by interchanging m_1 and m_2. This derivation is correct for all ϕ values for the uniaxial case $m_1 = m_2$. For $\phi \neq 0, \pi/2$, the problem is nontrivial, unless $m_1 = m_2$. We take the vector potential to be $\mathbf{A} = B(-y\cos\theta, 0, y\sin\theta)$. We then rotate[34] about the $\hat{\mathbf{b}}(\hat{\mathbf{y}})$ axis by θ, so that $\hat{\mathbf{c}} \to \hat{\tilde{\mathbf{c}}} = \hat{\mathbf{B}}$.

Under this rotation, k_z transforms like ∂_z, mixing with k_x. Note that the resulting potential is independent of x, so that $\tilde{\psi}$ may be written as

$$u(y)\exp[i(k_x x + k_z z)] = u(y)\exp[i(\tilde{k}_x \tilde{x} + \tilde{k}_z \tilde{z})] ,$$

invariant under the rotation. Hence, ∂_x and ∂_z behave as c numbers, in that they only operate upon $\exp(ik_x x)$ and $\exp(ik_z z)$ in the preceding expression for $\tilde{\psi}$. We thus have

$$\begin{aligned}\tilde{H}_n = {} & a(T)(i\partial_y)^2/2m_2 \\ & + [\cos\theta(2eBy - \tilde{k}_x) - \tilde{k}_z \sin\theta]^2/2m_1 \\ & + \bar{\lambda}_n\{s[(\sin\theta(2eBy - \tilde{k}_x) + \tilde{k}_z\cos\theta]\} \\ & + \delta\bar{\lambda}_n\{s[\sin\theta(2eBy - \tilde{k}_x) + \tilde{k}_z\cos\theta]\} . \end{aligned} \tag{14}$$

In what follows, we neglect $\delta\bar{\lambda}_n$, as we are primarily interested in the eigenvalues of $\tilde{H}_n$ to order B (see the Appendix). We note that the only $\tilde{k}_x$ dependence of $\tilde{H}_n$ is through the variable $2eBy - \tilde{k}_x$, so that $\tilde{k}_x$ can be eliminated by a shift in y: $2eBy - \tilde{k}_x \to 2eB\bar{y}$. The $\tilde{k}_z\cos\theta$ term inside the argument of $\bar{\lambda}_n$ could for $\theta \neq 0$ be removed by a shift in y, causing it to appear in the harmonic potential term. However, since we have already removed $\tilde{k}_x$, accounting for the Landau degeneracy, there is nothing to be gained by doing so.

Note that for $\theta = 0$, we recover the correct harmonic-oscillator Hamiltonian with a dispersion in the continuous degrees of freedom given by $\bar{\lambda}_n(sk_z)$, where $|k_z| \leq \pi/s$. For $\theta = \pi/2$, we obtain the expected Hill (or Mathieu, in the LD limit) equation, with a dispersion in the unbounded continuous degrees of freedom given by $k_x^2/2m_1$, exactly as in the crystal axis representation. As for the weak-field crystal axis representation calculation, there will not be any DCR to the 2D regime for $\theta = \pi/2$ in the temperature dependence of the SFD (as T is in-

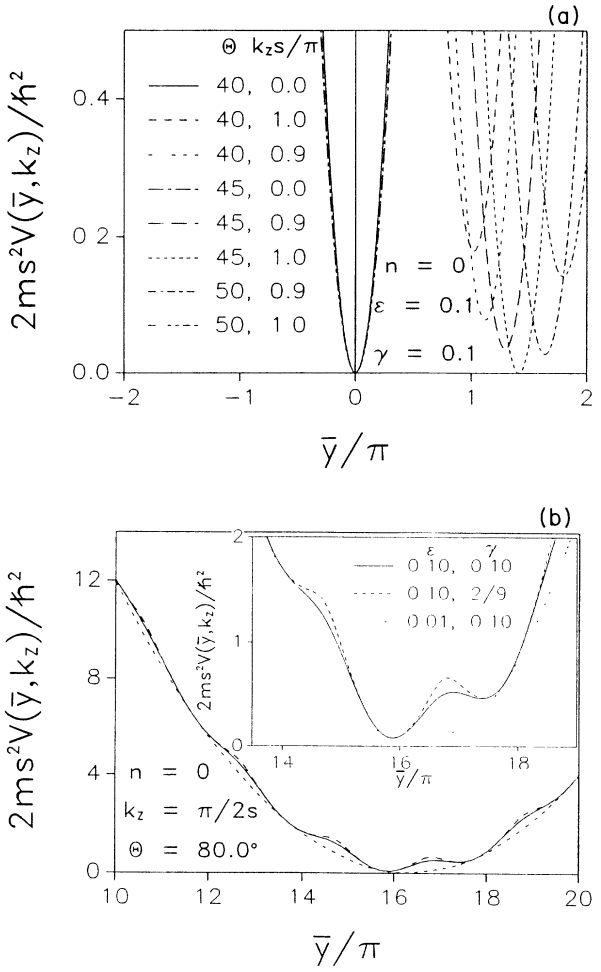

FIG. 6. (a) Plotted is the potential experienced by the quasihole pairs for field angles θ in the vicinity of 45°, as a function of the reduced real-space position $\bar{y}$, for various values of k_z. (b) Quasihole pair potential versus $\bar{y}$ for $\theta = 80°$ for $k_z = \pi/2s$. The case $\varepsilon = 0.01$, $\gamma = \frac{2}{9}$ is essentially identical to the $\varepsilon = 0.01$, $\gamma = 0.1$ case pictured.

creased from T_c), regardless of the band index n. Hence, Eq. (14) has the correct limiting behavior as $\theta \to 0$ and $\pi/2$.

Note that as $B \to 0$, the eigenvalues of the Hill (Mathieu) equation reduce to those of the harmonic oscillator, but deviate from them as B increases. Hence, for this direction of **B**, we would expect DCR in the field dependence of the SFD, similar to the DCR in H_{c2} below T_c for $\mathbf{B} \perp \hat{\mathbf{c}}$. We have estimated the crossover field B^* at which this occurs by expanding the lowest eigenvalue to order B^2, obtaining

$$B^* \sim 16(m_2/m_3)^{1/2}\phi_0/(\pi s^2) .$$

For Y-Ba-Cu-O, B^* is on the order of 240 T, making this difficult at best to observe. Hence, it is reasonable for $B \ll B^*$ to calculate the eigenvalues to order B (as in the weak-field case), but keeping account of the degeneracies of the eigenvalues, as discussed in the introduction to Sec. III. Since $s\tilde{k}_z\cos\theta$ is bounded by $\pm\pi$, this degeneracy only arises because the bounds upon $\bar{y}$ are $\pm L_\phi/2$.

Equation (14) further contains an additional very interesting feature: the presence of multiple potential minima, degenerate with the absolute minimum, for particular values of the field angle θ. To illustrate this important point as simply as possible, let us consider the case of an LD band, and let $\bar{y} = s(2eBy - \tilde{k}_x)$. Note that for $N=1$, $\delta\bar{\lambda}=0$. The potential in Eq. (14) can then be written as

$$V(\bar{y},\tilde{k}_z) = (\cos\theta\bar{y}/s - \tilde{k}_z\sin\theta)^2/(2m_1) + J[1-\cos(\bar{y}\sin\theta + s\tilde{k}_z\cos\theta)] , \quad (15)$$

which is ≥ 0. We recall that

$$-\tilde{k}_{z0} \leq \tilde{k}_z \leq \tilde{k}_{z0} = \pi/(s|\cos\theta|) .$$

At $\tilde{k}_z = 0$, the absolute minimum of $V(\bar{y},0)$ $(=0)$ occurs at $\bar{y}=0$. As $\tilde{k}_z$ is increased (decreased) from 0 to its maximum (minimum) value, $V(\bar{y},\tilde{k}_z)$ changes to

$$V(\bar{y},\pm\tilde{k}_{z0}) = (\cos\theta\bar{y} \mp \pi\tan\theta)^2/(2m_1s^2) + J[1+\cos(\bar{y}\sin\theta)] . \quad (16)$$

Since the two terms in V are both ≥ 0, another absolute minimum degenerate with the above one can only occur if both terms vanish. The first term vanishes for $\bar{y} = \pm\pi\sin\theta/\cos^2\theta$. With this value of $\bar{y}$, the second term $= J[1+\cos(\pi\tan^2\theta)]$, which vanishes at the set $\{\theta_m\}$ of discrete θ values given by

$$\theta_m = \tan^{-1}(2m-1)^{1/2}, \ n \text{ even} , \quad (17a)$$

where $m = 1,2,3,\ldots$ is a natural number. The preceding discussion can be easily generalized to arbitrary $\bar{\lambda}_n(q)$, and Eq. (17a) applies rigorously for n even. For n odd, we find

$$\theta_m = \tan^{-1}(2m)^{1/2}, \ n \text{ odd} . \quad (17b)$$

As θ is increased through θ_m, the magnitude of the SFD jumps almost discontinuously by a fraction $2/m$ of its value for $\theta < \theta_m$. This results in an angular dependence of $M_B(\theta,T)$ that resembles the field dependence of the dHvA effect. The appearance of one ($k_z = +\pi/s$) of the first secondary minima degenerate with the primary one is pictured in Fig. 6(a). We note that at $k_z = \pm\pi/s$, as θ is increased through 45°, the secondary minima are always higher in energy than the primary ($k_z = 0$) one, except exactly at 45°. The secondary potential minima never become lower in energy than the primary one. As H_{c2} is given by the lowest eigenvalue of the Hamiltonian, this means that this degeneracy has no effect whatsoever upon the angular dependence of H_{c2}. In the 3D regime just below T_c, $H_{c2}(\theta,\phi)$ is given by the usual anisotropic mass form.[34] Note that for $N>1$, these degeneracies are only exact to order B. For $N=2$, the $n=0$ degeneracies are also exact for the special case $\zeta_1 d = \zeta_2 d'$.

In Fig. 6(b), the potential for $\theta = 80°$ is pictured, showing that the potential is a tilted "washboard" potential, allowing for multiple (but nondegenerate) minima at the same k_z value. Note that in this case, there is a local maximum, which must be excluded from the region of integration, if one is to make the harmonic approximation about each of the minima.

In order to find the general θ dependence of the SFD, we write $\tilde{H}_n = T + V_n(\bar{y})$, where $T = (i\partial_{\bar{y}})^2/2m_2$, and V_n is the sum of the constant, harmonic, and periodic parts for the nth band. Since for both the $\theta=0$ and $\pi/2$ cases, V_n reduces to the harmonic-oscillator form for small B, it is reasonable to expect such behavior for arbitrary θ. To find the behavior in this limit, we expand $V_n(\bar{y})$ about its minimum value(s), which occur(s) at $\bar{y}^*$. We then have to solve the transcendental set of equations,

$$V_n(\bar{y}) \simeq a(T) + \bar{\lambda}_n(q^*) + (q^*\cos\theta - s\tilde{k}_z)^2/(2m_1s^2\sin^2\theta) + [2eB(\bar{y}-\bar{y}^*)]^2 a_n^2(\theta,q^*)/(2m_1) , \quad (18a)$$

$$q^* = s(2eB\bar{y}^*\sin\theta + \tilde{k}_z\cos\theta) , \quad (18b)$$

$$\cos\theta(q^*\cos\theta - s\tilde{k}_z) = -m_1s^2\sin^2\theta\bar{\lambda}_n'(q^*) , \quad (18c)$$

and

$$a_n^2(\theta,q^*) = \cos^2\theta + m_1s^2\sin^2\theta\bar{\lambda}_n''(q^*) > 0 , \quad (18d)$$

where the last relation is necessary to insure a minimum in the potential. We note that since $\bar{\lambda}_n(q^*)$ is periodic in q^*, Eq. (18c) is related to the problem of the metastability of the pinned charge-density wave condensate below threshold, and represents the minima of the "washboard" potential. In this context, it arises naturally from the periodic Josephson junction array of the layered superconductor. As expected, there are several regions of different behavior, arising from the presence of multiple minima.

Since Eq. (18a) is of the harmonic-oscillator form, the eigenvalues of the Hamiltonian may be found to order B exactly, yielding

$$\tilde{E}_{\tilde{k}_z np} = a(T) + \bar{\lambda}_n(q^*) + m_1s^2\tan^2\theta[\bar{\lambda}_n'(q^*)]^2/2 + (2p+1)eBa_n(\theta,q^*)/(m_1m_2)^{1/2} , \quad (19)$$

where we have used Eq. (18c).

We now may calculate the SFD. For $B/\tilde{H}_{c2}(\theta)\ll 1$, we calculate F/V to order B^2, where the Helmholtz free energy $F=-\beta^{-1}\ln(Z)$, $\beta=1/(k_BT)$, and Z is the partition function, obtaining $F/V\rightarrow f(\theta,\phi)B^2/2$ in the thermodynamic limit. The magnetization $\mathbf{M}=\hat{\mathbf{B}}M_{\mathbf{B}}+\hat{\theta}M_\theta+\hat{\phi}M_\phi$, where $M_{\mathbf{B}}=-\partial(F/V)/\partial B$, $M_\theta=-B^{-1}\partial(F/V)/\partial\theta$, and $M_\phi=(B\sin\theta)^{-1}\partial(F/V)/\partial\phi$, M_ϕ vanishing for uniaxial anisotropy. We define $\chi_{\mathbf{B}}\equiv M_{\mathbf{B}}/B$. Since F contains the Landau degeneracy factor (B/ϕ_0), it suffices to calculate $\tilde{E}$ to order B. From Z, we have

$$F/V=-[B/(\phi_0\beta)]\sum_{n=0}^{N-1}\sum_{p=0}^{\infty}\int_{-\tilde{k}_{z0}}^{\tilde{k}_{z0}}(d\tilde{k}_z/2\pi)\ln[\pi/(\beta\tilde{E}_{\tilde{k}_z np})]\ . \tag{20}$$

Differentiating F/V with respect to B, using the Poisson summation formula[20,30] (to calculate the sum over Landau levels), and integrating by parts (neglecting the wildly oscillating boundary terms in the usual fashion), we obtain,

$$\chi_{\mathbf{B}}=\frac{-\pi k_BT}{6\phi_0^2(m_1m_2)^{1/2}}\sum_{n=0}^{N-1}\int_{-\tilde{k}_{z0}}^{\tilde{k}_{z0}}\frac{d\tilde{k}_z a_n(\theta,q^*)\Theta(a_n^2(\theta,q^*))}{2\pi[a(T)+f_n(\theta,q^*)]}\ , \tag{21}$$

where

$$f_n(\theta,q^*)=\bar{\lambda}_n(q^*)+m_1s^2\tan^2\theta[\bar{\lambda}_n'(q^*)]^2/(2\hbar^2)\ , \tag{22}$$

and $\Theta(z)$ is the Heaviside step function. Using Eq. (18c) to change the integration variable from $\tilde{k}_z$ to q^*, we obtain,

$$\chi_{\mathbf{B}}=\frac{-\pi k_BTs}{12\phi_0^2|\cos\theta|m}\sum_{n=0}^{N-1}\int_{-q^*_{\max}}^{q^*_{\max}}\frac{dq^*a_n^3(\theta,q^*)\Theta(a_n^2(\theta,q^*))m_{3n}}{2\pi[Z_n^2+m_{3n}s^2f_n(\theta,q^*)/(2\hbar^2)]}\ , \tag{23}$$

where $q^*_{\max}$ is the maximum allowed solution of

$$\pi=q^*_{\max}\cos^2\theta+m_1s^2\sin^2\theta\bar{\lambda}_n'(q^*_{\max})/\hbar^2\ , \tag{24}$$

and $Z_n=s/[2\xi_{3n}(T)]$, where $\xi_{3n}(T)=(m/m_{3n})^{1/2}\xi_{ab}(T)$, $m=(m_1m_2)^{1/2}$, and $\xi_{ab}(T)=[2ma(T)]^{-1/2}$ is the geometric mean coherence length parallel to the layers. In Eqs. (22)–(24), we have reintroduced the quantity $\hbar$ for clarity. The integration region for positive q^* is pictured for relevant parameter values in Fig. 7. Note that near to $\theta=\pi/2$, there are many excluded regions, due to the restriction $a_n^2\geq 0$. An example of this was shown previously in Fig. 6(b).

We note that as $\theta\rightarrow 0$, $q^*_{\max}\rightarrow\pi$, leading to a $\chi_{\mathbf{B}}$ that reduces to the weak field form [Eq. (13c)]. In order to obtain Eq. (13a) for the weak-field $\theta=\pi/2$ result, one must introduce a cutoff in the q^* integration, such that no degeneracy is allowed, as already discussed. Letting $\gamma=\zeta_1\zeta_2/(\zeta_1+\zeta_2)^2$ as for weak fields, the LD form is obtained for $\gamma\rightarrow 0,\frac{1}{4}$. The maximum value of γ is $\frac{1}{4}$ by inspection. The $\bar{\lambda}_n$ can then be characterized in terms of the two parameters $\varepsilon=m/m_{30}$ and γ. The DCR temperature T_{0n} for the nth band is found by setting $Z_n^2[T_{0n}(\theta)]$ equal to the maximum allowed value of

$$m_{3n}s^2f_n(\theta,q^*)/2\ ,$$

yielding,

$$Z_n[T_{0n}(\theta)]=\max_{\{q^*\leq q^*_{\max}\}}\{m_{3n}s^2\bar{\lambda}_n(q^*)/2+m_1m_{3n}s^4\tan^2\theta[\bar{\lambda}_n'(q^*)]^2/4\}^{1/2}\ . \tag{25}$$

For $\gamma\rightarrow 0$ and $\theta\rightarrow 0$, this reduces to $Z_n[T_{0n}(\theta)]=1$, the familiar LD result. For $\gamma>0$, the values of $Z_n[T_{0n}(\theta)]$ are less than this, as pictured for $N=2$, $n=0$ in Fig. 8. We note that as $\gamma\rightarrow 0$, the $Z_0[T_{00}(\theta)]\rightarrow 1$ for $\theta\leq\theta_c$, where θ_c is the angle at which the first zero of $a_0^2(\theta,q^*)$ occurs. For $\gamma>0$, $Z_0[T_{00}(\theta)]$ is still a constant for $\theta\leq\theta_c$, but that constant decreases monotonically with increasing γ from 1 (for $\gamma=0$) to $1/\sqrt{2}$ (for $\gamma=\frac{1}{4}$). For $\theta>\theta_c$, $Z_0[T_{00}(\theta)]$ is less than this value, exhibiting a kink at θ_c. For $\varepsilon=0.1$, θ_c is found to be $\sim 71°$. As $\varepsilon\rightarrow 0$, $\theta_c\rightarrow 90°$. We note that in all cases, as $\theta\rightarrow 90°$, $Z_0(T_{00})\rightarrow 0$, implying no DCR for this field angle, even as $\varepsilon\rightarrow 0$, although in that special case, the DCR temperature jumps discontinuously from its $\theta=0$ value to ∞ at $\theta=90°$. Similar results are obtained for $n>0$, differing primarily in that the DCR temperature occurs at larger Z_n values.

Although in the interest of some degree of brevity, we have not shown the angular dependence of $\chi_{\mathbf{B}}$ in this static limit, Figs. 8–10 [which were calculated including dynamic effects] examined with a bit of imagination indicate that the special angles given by Eq. (17) appear dramatically in $\chi_{\mathbf{B}}(\theta,T)$. In addition, the lack of DCR is evident in $\chi_{\mathbf{B}}(\pi/2,T)$ in these figures. Note that for $n=1$, there is an additional broad maximum [not present in Eq. (17b)] at $\theta\simeq\pi/6$, since the curvature of the band is negative for small q^*. Except for this maximum in $\chi_{\mathbf{B}}(\theta)$ at fixed T, each of these θ_m values, an additional minimum

in the potential has become degenerate with the ground state. We note, however, that the denominator in Eq. (23) is only small for the $n=0$ band, so that the magnitude of the peaks for the upper bands is small relative to that of the $n=0$ band, unless T_{c1} is near to T_c. Curiously, if $T_{c1} \simeq T_c$, the peaks in the $n=1$ band will also be observable, and would be out of phase with the $n=0$ peaks.

Physically, the pairs move in orbits that are effectively extended beyond the first Brillouin Zone in the $\hat{c}^*$ direction (in the periodic zone scheme). This effective extension arises from the component of **B** in the *ab* plane, and has nothing to do with the rotation. We recall that the requirement for gauge invariance of the free energy introduced a phase difference proportional to A_3 between the OP's on adjacent layers. Since above T_c, **B** is a constant, A_3 varies linearly in position along the *ab* plane, giving rise to a pair potential that is periodic in real space. The origin of these peaks is due to a combination of the extension of the pair orbits beyond the first zone (by the magnetic field at the appropriate θ values) and to the presence of degenerate minima in the potential for these angles. If there were no cutoff (arising from finite-size effects or other mechanisms) in the maximum q^* value allowed, the orbits for $\theta=\pi/2$ would be truly open. Such was also the case for $\theta=\pi/2$ in the weak-field regime.

If no additional physical processes are introduced into the problem, $\chi_B(\pi/2,T)$ would be logarithmically divergent, for as θ is increased towards $\pi/2$, $\chi_B(\theta)$ would pick up contributions of relative weight $(2m-1)^{-1}$ from an infinite number of degenerate minima [see Fig. 6(a)]. We emphasize that this divergence arises solely from the infinite degeneracy of the energy levels for $\theta=\pi/2$ for finite fields, as already discussed. Hence, it is necessary to introduce a cutoff in q^* which is more stringent for θ near to $\pi/2$ than that given by Eq. (24). There are several possibilities for this cutoff, one of which has al-

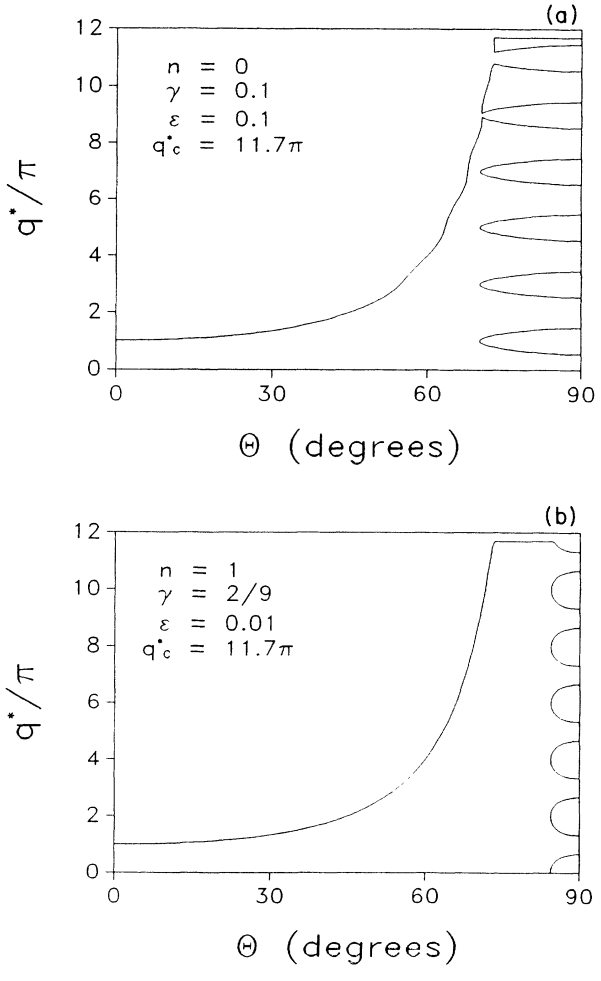

FIG. 7. Shown is the integration region for the high-field susceptibility calculation, as a function of the field angle θ. The ellipses centered at $q^*=(2p+1)\pi$ in (a) and $2p\pi$ in (b) are excluded, as they correspond to maxima in the potential. (a) $\varepsilon=0.01$, $\gamma=0.1$, $n=0$, $q_c^*=11.7\pi$; (b) $\varepsilon=0.01$, $\gamma=\frac{2}{9}$, $n=1$, $q_c^*=11.7\pi$.

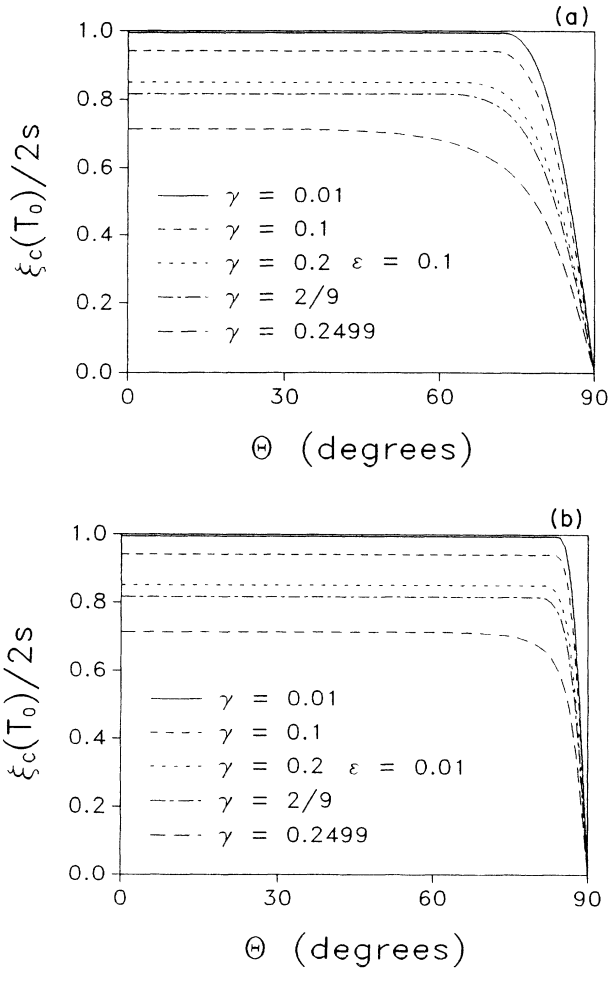

FIG. 8. Plotted is the high-field $\xi_c[T_0(\theta)]/2s$ vs θ for $n=0$ and several values of γ. (a) $\varepsilon=0.10$, (b) $\varepsilon=0.01$. The dimensional crossover temperature $T_0(\theta)$ is found from these curves combined with Eq. (29a) and $\xi_{30}(0)=\sqrt{\varepsilon}\xi_{ab0}(0)$. Note that $\xi_c(T)\equiv\xi_{30}(T)$.

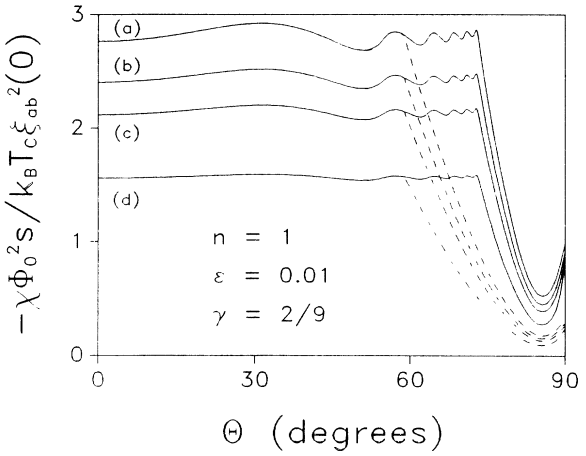

FIG. 9. Shown is a plot of the high-field $\chi_B(\theta)$ for $n=1, \varepsilon=0.01$, $\xi_{ab0}(0)=15$ Å and $\gamma=\frac{2}{9}$ at four temperatures. (a) $T/T_c=1.01$, (b) $T/T_c=1.07$, (c) $T/T_c=1.15$, and (d) $T/T_c=1.75$. The solid (dashed) lines are for $q_c^*=11.7\pi(3.74\pi)$, respectively.

ready been discussed somewhat in the introduction to Sec. III.

Assuming that the cutoff arises solely from physical processes present in the model, it would be due to the finite phase coherence length L_ϕ. As mentioned previously, for the field in the $\hat{\mathbf{a}}$ direction, the argument of the $\bar{\lambda}_n$ can range from sk_z-eBsL_ϕ to sk_z+eBsL_ϕ (for $-L_\phi/2<\bar{y}^*<L_\phi/2$). The degeneracy for that field angle and $B\neq 0$ was given by mod$[2eBsL_\phi/2\pi]$. This result can easily be extended to arbitrary θ, using Eq. (18b). Hence, for the finite-size cutoff, we have

$$q_c^*/\pi=(B/B_0)\sin\theta+1\ , \tag{26a}$$

where the one arises from the maximum value of $s\tilde{k}_z\cos\theta$, and $B_0=\phi_0/(sL_\phi)$. We note that $q_c^*\to\pi$ as $\theta\to 0$, and reduces to the correct finite-size cutoff as $\theta\to\pi/2$ discussed previously. In samples that are highly twinned or that exhibit many grain boundaries (such that $L_\phi/s\sim 10^2-10^3$), this phase coherence cutoff would likely be the dominant cutoff, except for very large B values. In large, perfect single crystals, however, we must consider other mechanisms, as this cutoff would diverge as $\theta\to\pi/2$ for $L_\phi\to\infty$.

Since q^*/s represents the allowed pair momentum values near the minima in the potential, it must be restricted by the allowed single quasihole momentum values, $\pm\mathbf{k}_F+\mathbf{q}^*/2s$, which depend upon the quasihole band structure and the $\mathbf{B}$ direction. Hence, we expect that if the single quasiholes are restricted to being in the first Brillouin zone (e.i., do not themselves move in extended orbits), the maximum q^* value would be on the order of

$$q_c^*=2sk_{F_{\min}}\ , \tag{26b}$$

where $k_{F_{\min}}$ is the minimum value of the Fermi momentum experienced by a quasihole moving in the presence of $\mathbf{B}$ at the angle θ. This cutoff is very sensitive to the precise details of the normal-state band filling, and could be strongly θ dependent. For $\theta=\pi/2$, we would expect (for a nearly half-filled band) $k_{F_{\min}}$ to be on the order of $\pi/2a$, where a is the 0-0 intralayer nearest-neighbor distance. Since for Y-Ba-Cu-O $\pi s/a\simeq 4.0\pi$, this would be sufficient to allow two peaks in the angular dependence of $\chi_B(\theta,T)$, and would be more stringent (for high-quality single crystals) than the phase coherence cutoff. In the figures presented in this paper, we have merely treated q_c^* as a constant, less than or on the order of $\pi s/a$. For aligned powders of Y-Ba-Cu-O, it is likely that the finite-size cutoff will predominate, especially for lower-field values. It should be noted, however, that q_c^* is proportional to s, so that this cutoff will be greatest for high-

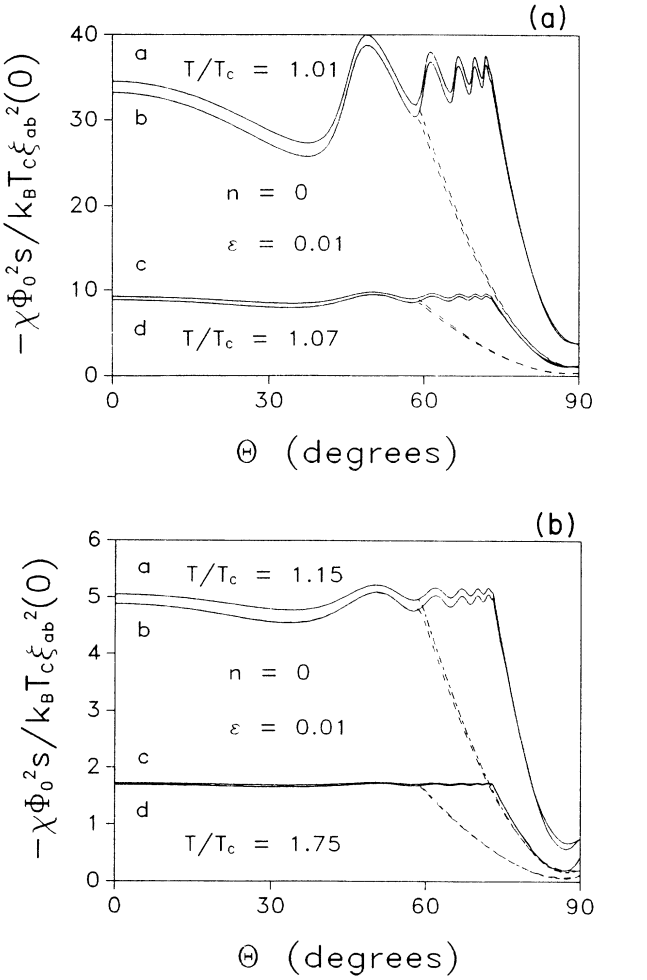

FIG. 10. Shown are plots of the high-field $\chi_B(\theta)$ for $n=0$, $\varepsilon=0.01$, $\xi_{ab0}(0)=15$ Å for two values of γ (0.01 and $\frac{2}{9}$), two values of q_c^*[11.7π, solid line, and 3.74π, dashed lines) at four temperatures. Upper: (a) $T/T_c=1.01$, $\gamma=\frac{2}{9}$; (b) $T/T_c=1.01$, $\gamma=0.1$; (c) $T/T_c=1.07$, $\gamma=\frac{2}{9}$; (d) $T/T_c=1.07$, $\gamma=0.1$. Lower: (a) $T/T_c=1.15$, $\gamma=2/9$; (b) $T/T_c=1.15$, $\gamma=0.1$; (c) $T/T_c=1.75$, $\gamma=\frac{2}{9}$; (d) $T/T_c=1.75$, $\gamma=0.1$.

quality materials with $N \geq 2$, and will increase with N.

We remark that while q_c^* depends upon θ, the question of whether the first peak (at $\theta_1 = \pi/4$) occurs or not really depends upon the value of $q_c^*(\theta_1)$, which must exceed 2π for the full peak to appear. If $\pi < q_c^*(\theta_1) < 2\pi$, a smaller rise, followed by a rapid decrease in $\chi_B(\theta)$ will occur near θ_1. If in some material, q_c^* were always well below 2π in magnitude, then $\chi_B(\theta)$ behaves in the 3D regime according to the anisotropic mass law, being proportional to $a_0^2(\theta,0)$. Curves for two arbitrarily chosen values of q_c^* are pictured in Figs. 9–13.

In Figs. 4 and 9–12, it can be clearly seen that the overall anisotropy $[\chi_B(0,T) - \chi_B(\pi/2,T)]$ in the high-field χ_B depends strongly upon the cutoff q_c^*. For $q_c^* < 2\pi$, $\chi_B(\theta)$ for the nth band closely approximates the

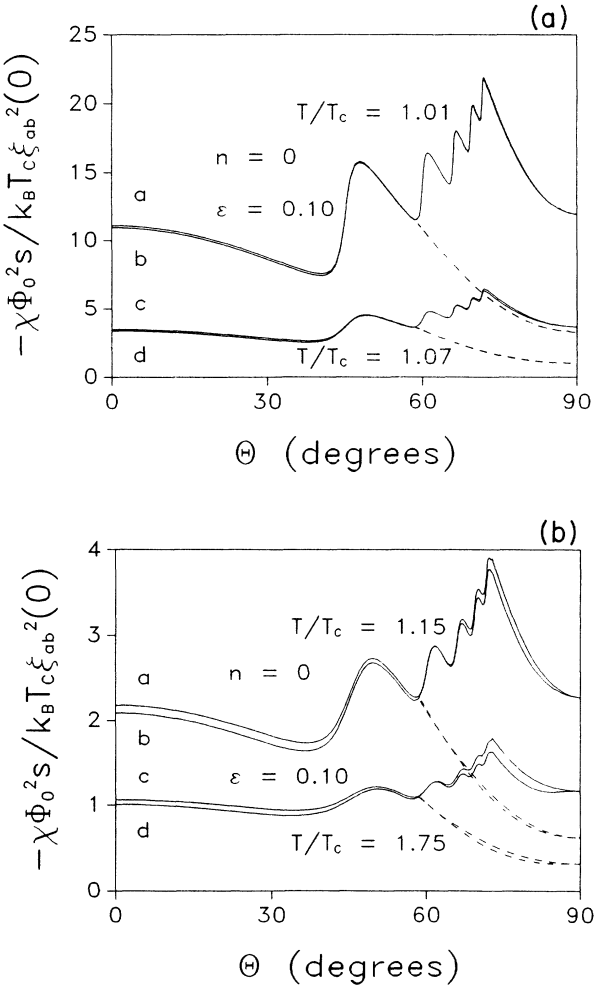

FIG. 11. Shown are plots of the high-field $\chi_B(\theta)$ for $n=0, \varepsilon=0.01$, $\xi_{ab0}(0)=15$ Å. The dashed (solid) lines are for $q_c^*=3.74\pi,(11.7\pi)$, respectively. Upper: (a) $T/T_c=1.01$, $\gamma=0.1$; (b) $T/T_c=1.01$, $\gamma=\frac{2}{9}$; (c) $T/T_c=1.07$, $\gamma=0.1$; (d) $T/T_c=1.07$, $\gamma=\frac{2}{9}$. Lower: (a) $T/T_c=1.15$, $\gamma=0.1$; (b) $T/T_c=1.15$, $\gamma=\frac{2}{9}$; (c) $T/T_c=1.75$, $\gamma=0.1$; (d) $T/T_c=1.75$, $\gamma=\frac{2}{9}$.

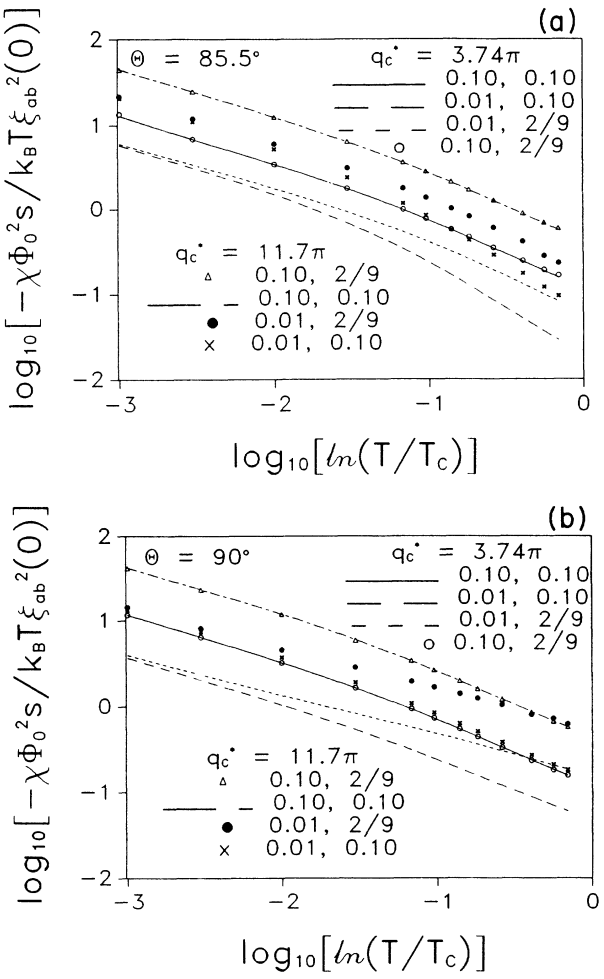

FIG. 12. Log-log plot of the high-field χ_B/T vs $\ln(T/T_c)$ for $\theta=85.5°$ and 90°, $\xi_{ab0}(0)=15$ Å. The legends indicate $\varepsilon, \gamma, q_c^*$ values (a) $\theta=85.5°$, (b) $\theta=90°$.

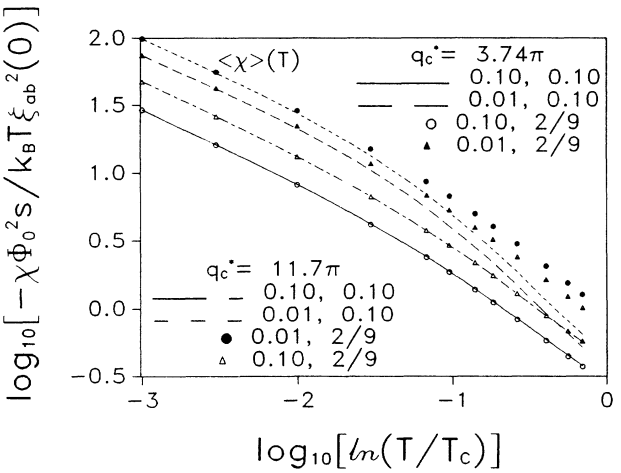

FIG. 13. Log-log plot of the high-field $\langle\chi_B\rangle/T$ vs $\ln(T/T_c)$ for $\xi_{ab0}(0)=15$ Å. The legends indicate $\varepsilon, \gamma, q_c^*$ values.

anisotropic mass form [$\chi_B(\theta) \sim a_n^2(\theta,0)$, as in the low-field regime] in the 3D regime. For $2\pi < q_c^* < 4\pi$, one anomaly is allowed, and the overall anisotropy in the 3D regime is considerably less (on the order of a factor of 3) than that of the anisotropic mass form. For larger q_c^* values, more anomalies are allowed, and the overall anisotropy can even be reversed in sign from the low-field value, even in the 3D regime, provided that ε and q_c^* are both sufficiently large, respectively. Hence, the presence of these extended orbits can drastically change the angular dependence of $\chi_B(\theta,T)$ from the anisotropic mass form, even in the 3D regime of the fluctuations!

We remark that as M_θ is proportional to $\partial\chi_B/\partial\theta$, maxima and minima in $\chi_B(\theta)$ will result in zeros for $M_\theta(\theta)$. In torque experiments, one measures $\mathbf{M}\times\mathbf{H}$, so the torque is proportional to M_θ. This would be in addition to the torque arising from the anisotropic Van Vleck susceptibility, which should have an angular dependence of the ordinary $\sin(2\theta)$ form, so one should look for oscillations on top of this background. In addition, if ζ_1 and ζ_2 were comparable, T_{c1} for the $n=1$ band (for $N=2$) would nearly equal T_{c0}.

IV. DYNAMIC EFFECTS UPON THE FLUCTUATION DIAMAGNETISM

As is well known for the dHvA effect, one would expect impurity scattering and the finite T to modify the sharpness of these anomalies. For the normal-state dHvA effect, one must have extremely clean samples and low T in order to observe any oscillations. The restrictions in that case arise from the Fermi-liquid nature of the normal state: At low T and high purity, the Landau levels do not overlap, and as the field is increased, successive Landau levels pass through the (sharp at low T) Fermi energy E_F. Finite T on the scale of E_F will smear the quasiparticle density of states as well as broaden the Landau levels.

For the SFD in the copper oxide superconductors, on the other hand, the temperature corresponding to $T=0$ in the dHvA effect is T_c. As for broadening of the levels, the relevant quantity is the phase coherence lifetime τ_ϕ. In this case, the overlapping of the Landau levels is less important, as the (pair) Landau levels are not to first approximation affected by the sharpness of the quasihole density of states near E_F. Rather, the peaks in $\chi_B(\theta)$ arise from the degeneracies at different k_z values in the pair potential. As already stated, there is good reason to believe $\tau_\phi k_B T_c/\hbar \gg \tau k_B T_c/\hbar \gtrsim 1$. We therefore believe the dominant broadening mechanism would be from the finite T (relative to T_c). This broadening will arise from fluctuations of the OP's in time, or dynamic effects. Since the microscopic pairing is thought to be local in nature, especially as the coherence lengths are so short (10–20 Å) within the planes, nonlocal effects will make at most a moderate modification to these results, provided[33] that $B/\tilde{H}_{c2}(0) \ll 1$.

To estimate the broadening of these anomalies, we have extended our calculation to the level of the time-dependent Ginzburg-Landau (TDGL) theory, using the clean limit for impurity scattering. The TDGL theory is also expected to give a much more accurate estimate of the fluctuations for T well above T_c; it is necessary to include these dynamic effects in order to obtain an accurate fit in the 2D regime. As we shall see in the following, quantitative deviations from the preceding static behavior are found to occur for T as near as 1 K from T_c, so that dynamic effects should also be included in comparison with the specific-heat data,[16] which extends roughly 10 K on either side of T_c.

We assume that the dynamic processes present in the Gaussian fluctuations are well approximated by the TDGL theory, modified to include N layers per unit cell. We assume that the OP ψ_{jn} relaxes according to

$$\frac{\delta F_s}{\delta \psi_{jn}^*} = -\eta_0\dot{\psi}_{jn} + \eta_1(\dot{\psi}_{j,n+1} + \dot{\psi}_{j,n-1}) = H\psi_{jn} \quad (n \neq N, 1) \tag{27a}$$

$$= -\eta_0\dot{\psi}_{jN} + \eta_1\dot{\psi}_{j,N-1} + \eta_2\dot{\psi}_{j+1,1} = H\psi_{jN} \quad (n = N) \tag{27b}$$

$$= -\eta_0\dot{\psi}_{j1} + \eta_1\dot{\psi}_{j,2} + \eta_2\dot{\psi}_{j-1,N} = H\psi_{j1} \quad (n = 1)\,, \tag{27c}$$

where η_0 describes the relaxation of ψ_{jn} due both to intralayer temporal processes and to the hopping of the pairs to the nearest-neighbor layers, and η_1, η_2 account for the corresponding increase in the OP's on the nearest-neighbor layers due to the hopping. For $N=1$, the η_1 process could be incorporated into the η_0 process, as all of the OP's have the same T_c value. For $N \geq 2$, one Fourier transforms $\psi_{jn}(t)$ to $\psi_{jn}(\omega)$, and then diagonalizes the resulting Hamiltonian exactly as in Sec. II, evaluating the resulting damping constants Γ_n at $q=\omega=0$ and at $T=T_{cn}$. The equation of motion for the nth OP $\tilde{\psi}$ (after the diagonalization) is thus given by

$$(i\omega + \Gamma_n \tilde{E}_{\tilde{k}_z np})\tilde{\psi}_{\tilde{k}_z np} = 0\,, \tag{27d}$$

where

$$\Gamma_n = 16m\xi_{abn}^2(0)k_B T_{cn}/\pi$$

in the clean limit[35] at T_{cn}. For $n=0$, Γ_0 is equivalent to $8/(\pi a_0)$, the standard result.[35] For $n \neq 0$, Γ_n is reduced from this value by the factor T_{cn}/T_c, as $\xi_{abn}(0)$ is assumed to reflect the range of the microscopic interactions, which we take to be nearly independent of n. For $N=2$, the $\xi_{abn}(0)$ are rigorously equal, but for $N \geq 3$, they are only approximately so. Therefore, we have henceforth kept the band index subscript associated with $\xi_{abn}(0)$.

We note that in a full BCS calculation, Γ_n becomes T dependent away from T_{cn}. To solve for the full T dependence of Γ_n, one would need to solve the microscopic model appropriate for N bands, which is analytically difficult. To incorporate this T dependence approximately, we multiply the respective contributions to the free energy from each of the bands by their respective Γ_n

values, in order to match the static calculation as $T \to T_c$. This has the effect of giving the various relaxation rates the same value at the highest T_c (T_{c0}). This procedure is shown explicitly in Sec. V.

The free energy now contains contributions from each of the fluctuating OP's, with $N(\omega)$ of them fluctuating at frequency ω, where

$$N(\omega)=1/[\exp(\beta\omega)-1]$$

is the boson occupation number. One must integrate the imaginary part of the inverse of the quantity in square brackets in Eq. (27) (i.e., the effective pair propagator) over the positive frequencies, weighted with the factor $N(\omega)+\frac{1}{2}$. For $\tau k_B T_c/\hbar \gtrsim 1$, however, the zero-point term gives rise to a large constant that is essentially B and T independent, and can be dropped, as first pointed out for bulk materials by Maki.[36] For dirty layered superconductors with the field in the $\hat{c}$ axis direction, the dropping of the zero-point term is also appropriate.[20,23] As it is likely that $10 > \tau k_B T_c/\hbar > 1$ for the materials of interest, we assume that the dropping of the zero-point term is a reasonable approximation.

We may then write down the expression for the high-field SFD that should be accurate over the entire T range of the measurement. We find,

$$\chi_B(\theta,T)=-\sum_{n=0}^{N-1}\frac{16k_B T_{cn}\xi_{abn}^2(0)}{3\pi^2 s|\cos\theta|\phi_0^2}\int_0^\infty\frac{\tilde{\omega}\,d\tilde{\omega}}{e^{\tilde{\omega}}-1}\int_0^{q^*_{\max}}\frac{dq^*a_n^3(\theta,q^*)\Theta(a_n^2(\theta,q^*))}{\tilde{\omega}^2+\bar{r}_n^2[Z_n^2+m_{3n}s^2f_n(\theta,q^*)/(2\hbar^2)]^2}\ , \tag{28}$$

where $\bar{r}_n=8r_n(T_{cn}/T)$, and $r_n=(4/\pi)[\xi_{3n}(0)/s]^2$ is the parameter introduced by KLB to characterize the degree to which DCR effects will enter into the "old" layered compounds.[20,23] In Eq. (28), we have set $\tilde{\omega}=\beta\omega$, so that both integration variables are in dimensionless units. We have also included $\hbar$ in the appropriate place, for clarification.

The low-field SFD can be found by modifying Eq. (13) in the same manner. Since $\chi_{zz}(T)$ (for weak fields) is identical to $\chi_B(0,T)$ (in high fields), χ_{zz} is given by Eq. (28) with $\theta=0$. By inspection,

$$\chi_{zz}(T)=\frac{-16}{3\pi^2 s\phi_0^2}\sum_{n=0}^{N-1}\int_0^\infty\frac{\tilde{\omega}\,d\tilde{\omega}}{e^{\tilde{\omega}}-1}\int_0^\pi\frac{dq\,k_B T\xi_{abn}^2(0)}{\tilde{\omega}^2+\bar{r}_n^2[Z_n^2+m_{3n}s^2\bar{\lambda}_n(q)/(2\hbar^2)]^2}\ . \tag{29a}$$

Log-log plots of the dynamic χ_{zz}/T versus $\ln(T/T_c)$ are given in Fig. 4, using the BCS form of $a(T)$ described in the following. Since χ_{yy} is given in terms of χ_{xx} by Eq. (13b), we need only find χ_{xx}. After integration over k_x, we find

$$\chi_{xx}=\sum_{n=0}^{N-1}\frac{-2m_1k_B(TT_{cn})^{1/2}\xi_{abn}^2(0)}{3\phi_0^2m_{3n}\xi_{3n}(0)\sqrt{\pi}}\int_0^\infty\frac{\tilde{\omega}d\tilde{\omega}\{[\tilde{\omega}^2+(\bar{r}_nZ_n^2)]^{1/2}-\bar{r}_nZ_n^2\}^{1/2}}{(e^{\tilde{\omega}}-1)[\tilde{\omega}^2+(\bar{r}_nZ_n^2)^2]^{1/2}}\ . \tag{29b}$$

Log-log plots of χ_{xx}/T versus $\ln(T/T_c)$ are given in Fig. 5, using Eq. (29) for the dynamic calculation, and the BCS form of $a(T)$ described in the following.

To properly take account of the different T_c values for the different bands as well as the BCS T dependence (arising from the digammalike functions in the clean-limit microscopic theory), we take the T dependence of ξ_{3n} to be

$$\xi_{3n}(T)=\xi_{3n}(0)|\ln(T/T_{cn})|^{-1/2}\ , \tag{30a}$$

where T_{cn} is not given by the oversimplified GL form above [Eq. (8), with $a(T)$ linear in $T-T_c$], but rather by the solution to

$$(T_{cn}/T_{c0})\ln(T_{c0}/T_{cn})=2m\xi_{abn}^2(0)\min[\bar{\lambda}_n(q^*)]\ . \tag{30b}$$

This definition of T_{cn} is consistent with Eq. (30a), but we must compensate for it in $\bar{\lambda}_n(q)$ [and hence $f_n(\theta,q)$] by the appropriate subtraction,

$$\bar{\lambda}_n(q)\to\tilde{\lambda}_n(q)=\bar{\lambda}_n(q)-\min_q[\bar{\lambda}_n(q)]\ , \tag{30c}$$

so that $a(T)+f_n(\theta,q)$ remains invariant under this redefinition of $\xi_{3n}(T)$.

We note that the difference in these logarithmic forms from the GL forms for $\xi_{3n}(T)$ is on the order of 10% in the vicinity of $2T_c$, so that it is important to use the preceding forms [Eq. (30)] in order to fit the data. The dynamic corrections as given by Eq. (28), make a substantial correction to the T dependence of the high-field static result at fixed θ [Eq. (23)], differing by more than a factor of 2 for $T\sim 2T_c$, as can be seen in Fig. 4(a) for $\theta=0$. The greatest correction to the T dependence of χ, however, is for weak fields and $\theta=\pi/2$, as can be seen in Fig. 5(a). In the static limit, $\chi_{xx}(T)/T$ fits a straight line with a slope of $-\frac{1}{2}$ on a log-log plot, but the dynamics cause χ_{xx} to decrease much more rapidly with increasing T, mimicing DCR behavior (which does not occur in this case). Hence, while it is considerably easier to use the simpler static form to fit the data, detailed fits should be performed with the full dynamic form. As we shall see in the following, this is also true for the fluctuation conductivity and FSH, unless one restricts the region of the measurement to a very narrow range near to T_c, and is not interested in DCR effects.

In Figs. 9–11, we have plotted the contributions to the high-field $\chi_B(\theta)$ from the upper (Fig. 9), and lower (Figs. 10 and 11) bands, for four values of T/T_c, two values of q_c^*, $\gamma=0.1$, and $\frac{2}{9}$, and for $\varepsilon=0.01$ and 0.1, respectively. For $N=2$, $\xi_{abn}(0)$ is independent of n. We note that the sharp rises present in the static limit are greatly smeared by the finite T. For $T/T_c=1.01$, the sharp rise is re-

duced (from a factor of 3 in the static limit) to a 20% rise near to θ_1, the T smearing changing the θ dependence of $\chi_B(\theta)$, as some weight from this peak is smeared out over a large angular region. In the 2D regime, the anomalies in $\chi_B(\theta)$ are still present, but further reduced in magnitude. In the absence of these peaks, the $\chi_B(\theta) \propto a_0^2(\theta,0)$ in the 3D regime, as for weak fields. Except for this finite T smearing, this simple anisotropic mass law is essentially obeyed in the high-field 3D regime for $\theta < \pi/4$.

In order to obtain a good fit to the data, it is necessary to limit the number of parameters as much as possible. Very recently, it was shown[27] that in aligned powders, the T dependence of the normal-state background could be eliminated by plotting the measured relative susceptibility

$$\chi_{zz}(T)-\chi_{xx}(T) \text{ [or } \chi_B(0,T)-\chi_B(\pi/2,T)] .$$

To measure the θ dependence of the high-field SFD, one should also fit to a relative susceptibility, such as $\chi_B(\theta,T)-\chi_B(\pi/2,T)$. This procedure is essential, as it was found[27] for weak fields that the normal-state background susceptibility bends down sharply as T_c is approached from above. In addition, Cu^{63} NMR data[3,4] are suggestive of a strongly T-dependent spin relaxation near to T_c.

In weak fields, there are the three parameters ε, γ, and $\xi_{ab}(0)$ to fit. In strong fields, q_c^* is also a fitting parameter, so that one would require measurements at a number of θ values. The parameter $\xi_{ab}(0)$ can be estimated from dc magnetization measurements of $\tilde{H}_{c2}(0)$. A recent measurement[19] has produced the value of 13.7 Å for $\xi_{ab}(0)$, for example. One could, in principle, use this procedure to determine ε, by comparing $\tilde{H}_{c2}(\pi/2)$ with $\tilde{H}_{c2}(0)$. However, one would need very strong fields (>50 T) to be able to determine $\tilde{H}_{c2}(\pi/2)$ accurately. This has not yet been done. Note that "irreversibility" problems[37] have often manifested themselves in a nonlinear $H_{c2}(T)$ curve near to T_c (obtained from ac susceptibility and/or resistivity measurements), even for $\theta=0$, making estimates from those published data unreliable. Another possible method of determining $\xi_{ab}(0)$ reliably is by a comparison of SFD and FSH data on the same sample, as we shall see in Sec. IV.

The effective mass anisotropy ε below T_c can also be estimated from dc magnetization measurements or torque measurements in the reversible intermediate state, leading to estimates[38] for Y-Ba-Cu-O of $\varepsilon \simeq 0.04-0.06$. These results are consistent with lower critical field H_{c1} measurements[39] on Y-Ba-Cu-O. As we shall see in Sec. V, however, there is at least a reasonable doubt as to whether those low-T values ought to apply above T_c. The best procedure to determine the values above T_c is to base the determination solely upon measurements done above T_c.

In Fig. 4(a), we have provided log-log plots of $\chi_B(0,T)/T[=\chi_{zz}(T)/T]$ versus $\ln(T/T_c)$ for the parameters used in Figs. 9–11. At this θ value, χ_B is independent of the cutoff q_c^*. We have also shown the same calculation in the static limit, in order to indicate precisely the degree to which the static calculation can be trusted. Near to T_c, the static calculation is not too bad, but consistently exceeds the dynamic calculation in the experimentally accessible regime ($T/T_c > 1.01$). On a log-log plot, the apparent slope of $\log_{10}(-\chi_{zz}/T)$ vs $\log_{10}[\ln(T_c)]$ is steeper in the experimentally accessible regime [e.g., outside the critical region] than the static result of $-\frac{1}{2}$, being on the order of -0.55 to -0.65, depending upon the parameter values. For $\varepsilon=0.01$, $\gamma=\frac{2}{9}$, the $n=1$ band has a T_{c1} value of 0.78 T_c, and contributes substantially to the 2D regime of χ_{zz}. In Fig. 4(b), we have presented additional curves for $\xi_{ab}(0)$ values of 10 and 20 Å, respectively, using only the dynamic theory. For $\xi_{ab}(0)=20$ Å the T_{c1} value of the $n=1$ band for $\varepsilon=0.01$, $\gamma=\frac{2}{9}$ is shifted down to 0.45 T_c, and makes less of a contribution to the 2D regime of χ_{zz}. For $\xi_{ab}(0)=10$ Å, the T_{c1} value for $\varepsilon=0.01$, $\gamma=\frac{2}{9}$ is shifted up to 0.90 T_c, and for $\varepsilon=0.01$, $\gamma=0.1$, it is 0.68 T_c, so the $n=1$ band contributes substantially to the 2D regime, even for this small γ value. In Figs. 5(a) and 5(b), log-log plots with the same parameters are given for $\chi_{xx}(T)/T$ versus T, as discussed previously. In this case, the static results are greatly modified by the dynamic corrections.

In Figs. 12(a) and 12(b) we have provided log-log plots of the high-field χ_B/T versus $\ln(T/T_c)$ for field angles in the vicinity of $\pi/2$. At $\theta=85.5°$, DCR for $\varepsilon=0.01$ is still present [see Fig. 6(b)]. At $\theta=90°$, the numerical calculation is difficult; we therefore made quadratic extrapolations from the values 86.4°, 87.3°, 88.2°, and 89.1°, respectively. The results of these calculations extrapolated to 90° are presented in Fig. 12(b). We note that while $\chi_B(\pi/2,T)$ does not exhibit any DCR effects, the slope of $\log_{10}(-\chi_B/T)$ versus $\log_{10}[\ln(T/T_c)]$ curve does bend downward, as in the low-field case pictured in Fig. 5. In both field regimes, this downward bending is not due to DCR effects, but rather to dynamic effects.

An additional point of note is that the slope of the two curves with $n=1$ bands exhibiting nonvanishing T_c values is greatly affected in the high-T regime, even though the effective dimensionality is 3 for this direction. In particular, at $\theta=\pi/2$, the high-field $\chi_B(\pi/2,T)$ is very sensitive to q_c^*, so that this angle ought to be studied carefully in high fields in order to limit the range of possible q_c^* values.

Since most of the experiments to date have been performed on unaligned powders, in Fig. 13 we have presented the powder average calculation in a similar log-log plot of the high-field SFD. We note that the powder average is sensitive not only to ε, γ, and $\xi_{ab}(0)$ (the variation with which is not pictured here), but also strongly dependent upon q_c^*.

V. FLUCTUATION SPECIFIC HEAT

We now turn to the fluctuation specific heat (FSH). Compared to the SFD, the FSH in zero field is elementary to calculate. For bulk superconductors, the static calculation near to T_c for a single band material has been given by Aslmazov and Larkin.[40] This is easily generalized above T_c to the case of multiple OP bands and to include the dynamic processes. As the FSH is given by

$C=-T(\partial^2/\partial T^2)(F/V)$ in zero field, one has merely to find the eigenvalues in zero field, write the expression for the Helmholtz free energy, and differentiate it twice with respect to T. In zero field, the complications of multiple minima (and hence q_c^*) do not arise, as the eigenvalues are simply given by

$$E_n(k_\parallel,k_z)=\sum_{\mu=1,2} k_\mu^2/(2m_\mu)+a(T)+\bar{\lambda}_n(sk_z) . \quad (31)$$

The fluctuation free energy can be written as a sum over the logarithm of the pair propagator, which in our notation becomes

$$F=-(2/\pi)\sum_{n=0}^{N-1}[8/(\pi\Gamma_n)]^2\int_0^\infty d\omega\, N(\omega)\int_{-\infty}^{\infty} d^2k_\parallel \times\int_{-\pi/s}^{\pi/s} dk_z(2\pi)^{-3}\mathrm{Im}[\ln(D)] , \quad (32a)$$

where

$$D^{-1}=i\omega+\Gamma_n E_n(k_\parallel,k_z) . \quad (32b)$$

As mentioned in the preceding section, the factor $(8/\pi\Gamma_n)^2$ is inserted to approximate the T dependence of Γ_n, and is necessary in this TDGL approach in order that the FSH reduce to the static result very near to T_c. The FSH above T_c is then given by taking two derivatives with respect to T of Eq. (32). Note that the usual Aslamazov-Larkin term involves both derivatives acting upon the pair propagator, but there is an additional term (which is not divergent near to T_c) obtained by differentiating the propagator only once. To obtain a reliable form for the FSH far from T_c, we have investigated this extra term as well.

After differentiation with respect to T, it is then possible to simplify Eq. (32) by first performing the integrals over k_1 and k_2, before taking the imaginary part of the quantity in curly brackets, as in the static case. This can be done by letting

$$x_\mu=k_\mu[\Gamma_n/(2m_\mu)]^{1/2} ,$$

and using polar coordinates $[x_1=\rho\cos\eta, x_2=\rho\sin\eta]$. The integrals over η and ρ can then be done by inspection. Transforming to $\tilde{\omega}$ as for the SFD, we obtain an expression for $C^+(T)$, accurate in both the 3D and 2D regimes,

$$C^+(T)=\sum_{n=0}^{N-1}\frac{4k_B T_{cn}}{\pi^4 s\xi_{abn}^2(0)T}\times\int_0^\infty\frac{d\tilde{\omega}}{e^{\tilde{\omega}}-1}\int_0^\pi dq[f_1(\Omega_n,q)+\Xi f_2(\Omega_n)] , \quad (33a)$$

where

$$f_1(x,q)=x/[(x^2+1)Y_n(q)] , \quad (33b)$$

$$f_2(x)=\tan^{-1}(x) , \quad (33c)$$

$$Y_n(q)=\bar{r}_n[Z_n^2+m_{3n}s^2\tilde{\lambda}_n(q)/(2\hbar^2)] , \quad (33d)$$

$$\Omega_n=\tilde{\omega}/Y_n(q) , \quad (33e)$$

and

$$\Xi=\hbar^2/(2m_{3n}s^2\bar{r}_n k_B T_{cn}) . \quad (33f)$$

We note that Ξ is typically on the order of 10^{-2}, and that $f_2(x)$ is bounded by 0 and $\pi/2$ in magnitude. Hence, the inclusion of the additional term proportional to Ξ only makes at best a correction on the order of 1%, even in the 2D regime. Henceforth, we shall neglect it. Equation (33) reduces to the LD form obtained recently by Quader and Abrahams[41] in the static limit as $\gamma\to 0$. [Note that we have put $\hbar$ back into Eq. (33).] Recall that $\tilde{\lambda}_n(q)$ and the $\xi_{3n}(T)$ present in $Z_n[=s/(2\xi_{3n})]$ are given by Eqs. (30c) and (30a), respectively.

Below T_c, only the $n=0$ band (with the highest T_{cn} value) survives in the Gaussian regime. We may expand about the mean-field solution to calculate $C^-(T)$ arising from the Gaussian fluctuations below T_c,

$$C^-(T)=\frac{2k_B T_c}{\pi^4 s\xi_{ab-}^2(0)T}\int_0^\infty\frac{\tilde{\omega}\,d\tilde{\omega}}{e^{\tilde{\omega}}-1}\int_0^\pi\frac{dq}{\tilde{\omega}^2+\bar{r}_0^2[Z_-^2+m_{30}s^2\bar{\lambda}_0(q)/(2\hbar^2)]^2} , \quad (34)$$

where $\xi_{ab-}(0)=\xi_{ab0}(0)/\sqrt{2}$, $Z_-=s/(2\xi_{3-})$, and $\xi_{3-}(T)=\xi_{30}(T)/\sqrt{2}$. If only the $n=0$ band were present above T_c, $C^-(T)$ would exceed $C^+(T)$ at fixed $|T-T_c|$ in the 3D regime by the factor $2^{1/2}$, due to differences in the coherent volume and the freezing of half of the degrees of freedom. However, the suppression of T_{cn} for $n\neq 0$ from the mean-field value to zero reduces the overall amplitude of $C^-(T)$ below T_c.

In order to properly fit the specific-heat data near to T_c, it is essential to ensure that the superconducting transition be second order, or else the entire BCS picture would break down. This implies that the total entropy change ΔS during the transition from the normal to the superconducting state must equal 0. In conventional superconductors, the entropy associated with the fluctuations is negligible, as the zero-temperature coherent volume $\xi_1(0)\xi_2(0)\xi_3(0)$ (appearing in the denominator of $C^\pm(T)$ in the 3D regime near to T_c) is sufficiently large that the fluctuation entropy can be safely ignored in computing ΔS for the transition. For the copper oxide superconductors, however, this coherent volume is on the order of 100–500 Å,[3] which is at least three orders of magnitude smaller than in conventional materials. Hence, a self-consistent fit to the data must include the nonvanishing fluctuation entropy, and treat the mean-field (BCS) entropy of the transition as nonvanishing. There are many ways to do this,[42] but the procedure we suggest below is the simplest one of which we are aware.

We assume that the normal-state density of states $\tilde{N}(0)$ at the Fermi level below T_c is less than that above

T_c,$N(0)$. This change in the density of states is not necessarily discontinuous; it could occur over a T range of a few K about T_c. As the electronic specific heat of the normal state above T_c is assumed to be of the usual form γT, where $\gamma \propto N(0)$, we assume that the (modified) BCS mean-field form of the specific heat below T_c is characterized by the parameter $\tilde{\gamma} < \gamma$, where $\tilde{\gamma}/\gamma = \tilde{N}(0)/N(0)$. Just below T_c, we may then use the BCS form for the mean-field specific heat (computed by Mühlschlegel[43]), with the preceding modification,

$$C_{\rm mf}(T) = \gamma T \Theta(T - T_c) + \Theta(T_c - T)[2.43\tilde{\gamma} T_c + 4.76\tilde{\gamma}(T - T_c) + \cdots] . \quad (35)$$

This reduces the BCS weak-coupling specific-heat jump at T_c from the usual $1.43\gamma T_c$ to $(2.43\tilde{\gamma} - \gamma)T_c$. Hence, the effective entropy conservation equation becomes

$$\int_0^{T_c} dT\, C^-(T)/T + \int_{T_c}^{T_{\max}} dT\, C^+(T)/T + \tilde{\gamma} T_c = \gamma(T_{\max} - T_c) , \quad (36)$$

where $T_{\max}(> T_c)$ is the maximum T for which the fit is to be performed. Due to the uncertainty in the experimental background (due to contributions from phonons, etc.), $T_{\max}$ is most likely to be limited to the range 1.1–1.2 T_c. In addition, we must be a bit careful in calculating the fluctuation contribution to the entropy below T_c, as our expression, [Eq. (34)] breaks down as $T \to 0$. Hence, we should place a low-T cutoff on the first integral in Eq. (34) at $T_{\min}$ (roughly 0.1–0.2 T_c), below which we expect $C^-(T)$ to be proportional to

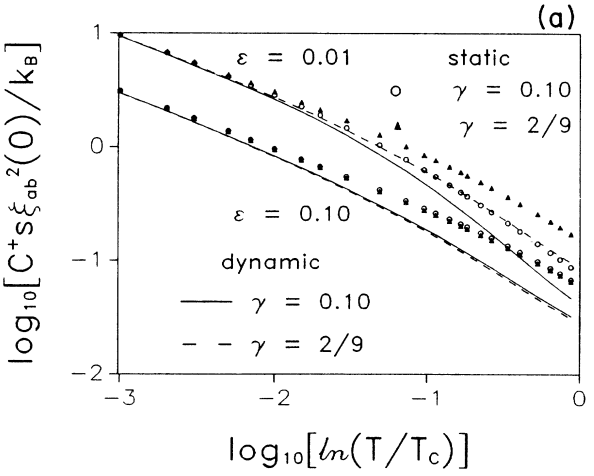

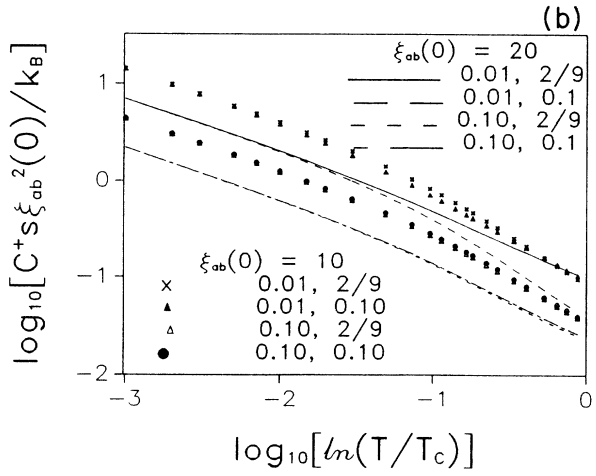

FIG. 14. Log-log plots of C^+ vs $\ln(T/T_c)$ for $\varepsilon = 0.1$ and 0.01; $\gamma = 0.1$ and $\frac{2}{9}$. (a) $\xi_{ab0}(0) = 15$ Å. The open circles and solid triangles are the result of the static approximation; solid and dashed lines are dynamic results for the same parameters. (b) $\xi_{ab0}(0) = 20$ and 10 Å. The legends indicate the ε and γ values. All calculations are dynamic ones.

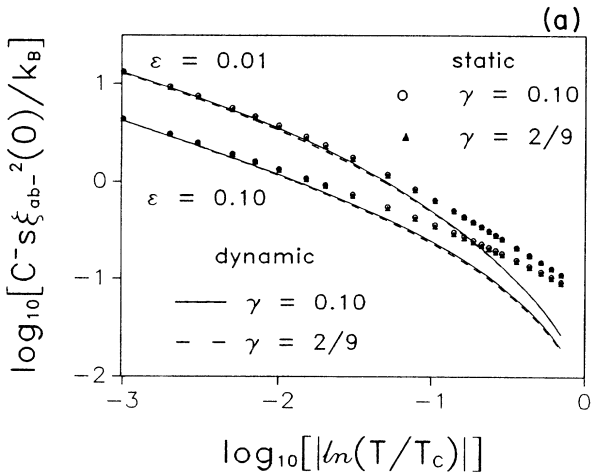

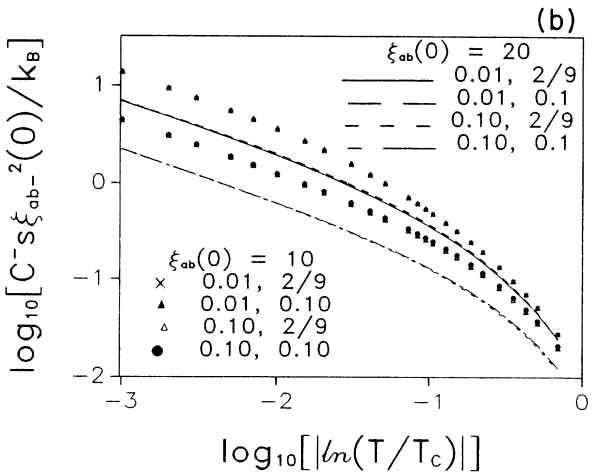

FIG. 15. Log-log plots of C^- versus $\ln(T/T_c)$ for $\varepsilon = 0.1$ and 0.01; $\gamma = 0.1$ and $\frac{2}{9}$. (a) $\xi_{ab0}(0) = 15$ Å. The open circles and solid triangles are the results of the static approximation. The solid and dashed lines are dynamic results for the same parameters. (b) $\xi_{ab0}(0) = 20$ and 10 Å. The legends indicate the ε and γ values. All calculations are dynamic ones.

$\exp[-\Delta(0)/T]$. As the dominant contribution to the fluctuation entropy arises from the temperature range near to T_c, the calculated fluctuation entropy should not be particularly sensitive to either $T_{\max}$ or $T_{\min}$.

One might think that it is somewhat unappealing to have the normal-state density of states change essentially discontinuously at T_c. However, there does seem to be some experimental evidence[44] for a first-order transition in the normal-state properties at T_c, so this assumption is probably not too bad. We reiterate that it is only necessary for the normal-state properties to change in the fluctuation regime. It is still possible to construct a Ginzburg-Landau and a BCS theory with parameters analytic in T at and near to T_c, but changing rapidly in that regime. Hence, the effective mass anisotropy could be essentially constant over most of the $T > T_c$ fluctuation regime, change rapidly near to T_c, and be essentially constant (with a different value) below T_c. In fits to the FSH, one should allow for this possibility, in order that the fit be fully self-consistent. It seems to us that the effective mass anisotropy obtained from the torque[38] and H_{c1} measurements[39] should be used in the fits below T_c, but not above T_c.

In addition, since we are not aware of any experimental data to date, that has definitively exhibited an actual specific-heat divergence at T_c, it is further essential to include a distribution of T_c values in the fit, or else incorporate a crossover into the critical regime. Such a T_c distribution should also be included in fits to the SFD and the fluctuation conductivity, especially for the data points near to T_c. In the very recent data of Inderhees *et al.*,[16] a very sharp transition was observed, suggestive of a crossover into the critical regime, as the nondivergence could not be fit to a spread in T_c values.

In Fig. 14, we have presented log-log plots of $C^+(T)$ versus $\ln(T/T_c)$. In Fig. 14(a), the static approximation is also shown, indicating that even for T as low as 1 K above T_c, the apparent power law divergence differs from the static result substantially. We note that Fig. 14(a) is very similar to Fig. 11(a), and that Fig. 14(b) is very similar to Fig. 11(b). Examination of Eqs. (28) and (33a) shows why this is so. Even for situations in which the upper band(s) enter into the calculation, $\chi_{zz}(T)/T$ is proportional to $C^+(T)$,

$$\chi_{zz}(T)/T = [4\pi^2 \xi_{ab}^4(0)/3\phi_0^2] C^+(T) , \tag{37}$$

assuming only that the $\xi_{abn}(0)$ are independent of n (rigorous for $N=2$). Hence a measurement of $\chi_{zz}(T)$ and $C^+(T)$ on the same sample should aid in determining the backgrounds present in each measurement, as well as give an accurate measure of $\xi_{ab}(0)$. Once the backgrounds are determined, fits of $C^+(T)$ and $\chi_{zz}(T)/T$ to the data should determine ε. We note that the inverse power of T on the left-hand side of Eq. (37) arises from using the BCS form of $a(T)$ [the Ginzburg-Landau form $a_0(T-T_c)$ would result in the T appearing in the numerator of the left-hand side].

In Fig. 15, we have presented a log-log plot of $C^-(T)$ versus $\ln(T/T_c)$. Although the approximation used here is not expected to be valid at the lowest T pictured ($0.5T_c$), there are some features which we believe to be intrinsic that are exhibited. We note that since the upper band does not contribute to the Gaussian fluctuations below T_c, the variation of the curves with γ is less striking than above T_c. In addition, it appears that the approximation of keeping only the leading two terms in the free energy expansion in even powers of the OP may not be too bad, as the dynamic calculation indicates that the fluctuations fall rapidly in magnitude as T is lowered below $\simeq 0.9T_c$, which we would expect, even for a correct static calculation involving the proper treatment of the mean-field solution in this region.

We note that near to T_c, $C^{\pm}(T) \propto [\xi_{ab}^2(0)\xi_3(0)]^{-1}$, so that a comparison of Figs. 14 and 15 near to T_c shows a discontinuity in the plots of nearly $\sqrt{2}$ due to the way in which we have plotted the curves.

VI. FLUCTUATION CONDUCTIVITY

We now turn to the fluctuation conductivity. In our model, the absence of an explicit appearance of impurity scattering precludes an accurate treatment of the Maki-Thompson diagrams.[45] We note that these diagrams do not arise directly from the free energy, but are known to be important in the case of thin films. A full treatment of the Maki-Thompson diagrams should be performed from the starting point of a microscopic calculation, involving the single quasihole scattering rate $1/\tau$. One would then have to calculate the free energy derivable (Aslamazov-Larkin) diagram on an equal basis. As we shall see in the following, any calculation of the Maki-Thompson diagrams cannot be trusted more than a few degrees above T_c, unless it takes full account of the dynamics.

We have seen that dynamical corrections play an important role in the fits to the SFD and FSH data, especially for $T/T_c > 1.01$. As the conductivity is relatively easy to measure far from T_c, and as preliminary investigations have used the LD (static) model to fit their data, their conclusions that DCR behavior was observed were premature, as the theory was only accurate very near to T_c. Hence, we have calculated the fluctuation conductivity for our model, keeping only the Aslamazov-Larkin[40] term, which can be derived directly from the fluctuation free energy. We have extended the LD model to include multiple layers per unit cell, and have included the clean-limit dynamics, precisely as for the SFD and the FSH. As for the FSH, we have only treated the case $B=0$. The case of a strong applied magnetic field is very interesting, as one would expect from the preceding discussion of the high-field SFD. Since this Aslamazov-Larkin term[40] and the SFD are both derived from the free energy, the fluctuation magnetoresistance in a strong field ought to exhibit oscillations in the field angle θ (relative to the $\hat{c}$ axis), similar to Shubnikov–de Haas oscillations.

In their classical paper, Aslamazov and Larkin[40]

showed how to derive the fluctuation conductivity microscopically, including dynamic effects. However, the results they derived analytically were only for the static limit [obtained by approximating $\exp(\beta\omega)$ by $1+\beta\omega$ in the internal integration frequencies], valid very near to T_c. Following their derivation, we use the clean, local limit as above, and obtain the static (i.e., dc) fluctuation conductivity $\sigma_{\alpha\beta}$ in zero field,

$$\sigma_{\alpha\beta}=(4/\pi)\sum_{n=0}^{N-1}\int_0^\infty \omega N(\omega)d\omega\int d^3k\ \Lambda_\alpha\Lambda_\beta\Gamma_n^2(2\pi)^{-3}\{(\Gamma_n^2E_n^2-\omega^2)/[(\Gamma_n^2E_n^2+\omega^2)^3]\}\ , \tag{38a}$$

where

$$\Lambda_\mu=2ek_\mu/m_\mu \quad \text{for } \mu=1,2 \tag{38b}$$

and

$$\Lambda_3=2es\bar{\lambda}'(k_zs)\ , \tag{38c}$$

and where $E_n(k_\parallel,k_z)$ and Γ_n are given by Eq. (31) and in the sentence following Eq. (27), respectively. In Eq. (37a), it is understood that the integration over k_μ is unrestricted for $\mu=1,2$, but the integration over k_z is restricted to those values not exceeding π/s in magnitude. As for the specific heat, it is possible to perform the integrations over k_1 and k_2 exactly, using the same procedure as above. we find $\sigma_{\alpha\beta}=\sigma_{\alpha\alpha}\delta_{\alpha\beta}$, where

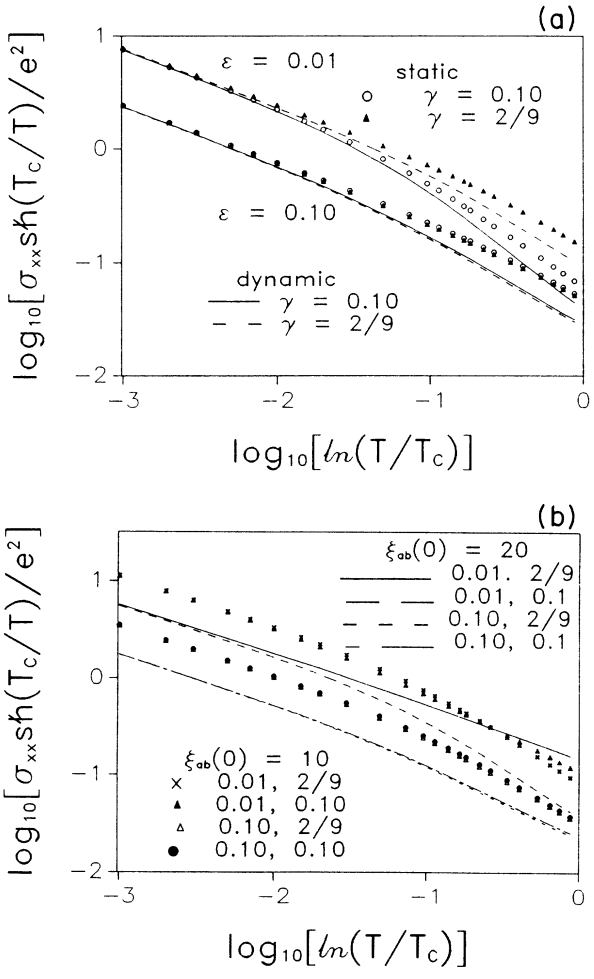

FIG. 16. Log-log plots of σ_{xx}/T vs $\ln(T/T_c)$ for $\varepsilon=0.1$ and 0.01; $\gamma=0.1$ and $\frac{2}{9}$. (a) $\xi_{ab0}(0)=15$ Å. The open circles and solid triangles are the results of the static approximation. The solid and dashed lines are the full dynamic results for the same parameters. (b) $\xi_{ab0}(0)=20$ and 10 Å. The legends indicate the ε and γ values. All calculations are dynamic ones.

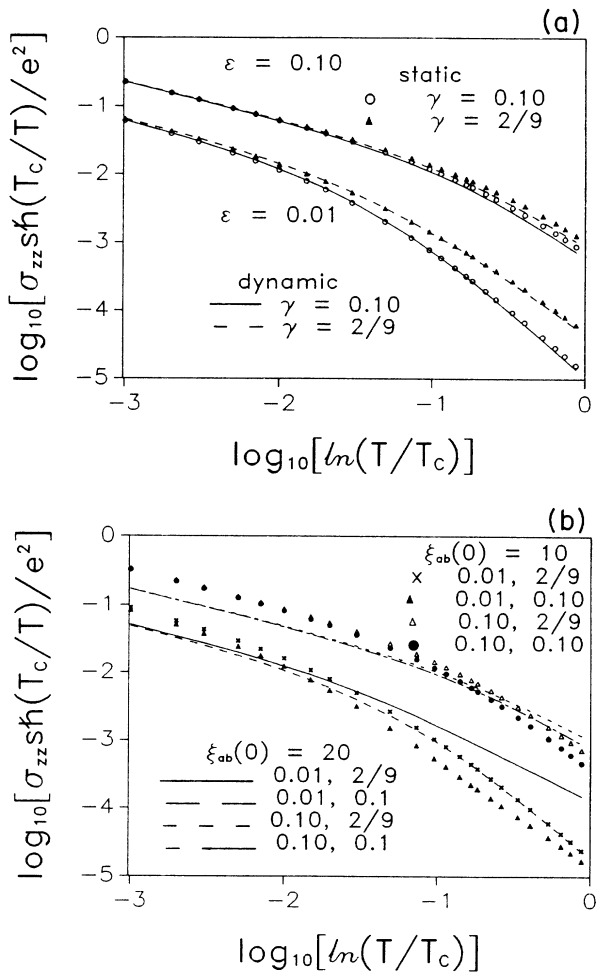

FIG. 17. Log-log plots of σ_{zz}/T vs $\ln(T/T_c)$ for $\varepsilon=0.1$ and 0.01; $\gamma=0.1$ and $\frac{2}{9}$. (a) $\xi_{ab0}(0)=15$ Å. The open circles and solid triangles are the results of the static approximation. The solid and dashed lines are the full dynamic results for the same parameters. (b) $\xi_{ab0}(0)=20$ and 10 Å. The legends indicate the ε and γ values. All calculations are dynamic ones.

$$\sigma_{xx}=\frac{2e^2(m_2)^{1/2}}{\pi^3 s\hbar(m_1)^{1/2}}\sum_{n=0}^{N-1}\int_0^\infty\frac{\tilde{\omega}\,d\tilde{\omega}}{e^{\tilde{\omega}}-1}\int_0^\pi\frac{dq f(\Omega_n)}{\bar{r}_n^2[Z_n^2+m_{3n}s^2\tilde{\lambda}_n(q)/(2\hbar^2)]^2}\ , \tag{39a}$$

$$\sigma_{yy}=(m_1/m_2)\sigma_{xx}\ , \tag{39b}$$

and

$$\sigma_{zz}=\frac{e^2m}{\pi^3 s\hbar}\sum_{n=0}^{N-1}\int_0^\infty\frac{\tilde{\omega}\,d\tilde{\omega}}{e^{\tilde{\omega}}-1}\int_0^\pi\frac{dq\, m_{3n}s^4[\bar{\lambda}_n'(q)]^2 g(\Omega_n)}{\hbar^2\bar{r}_n^2[Z_n^2+m_{3n}s^2\tilde{\lambda}_n(q)/(2\hbar^2)]^3}\ , \tag{39c}$$

where

$$f(x)=[\tan^{-1}(x)-x/(1+x^2)]/x^3\ , \tag{39d}$$

$$g(x)=2/(1+x^2)^2-f(x)\ , \tag{39e}$$

and Ω_n is given by Eqs. (33d,e). Note that in Eq. (39) we have reinserted the quantity $\hbar$, in order that the expressions have the appropriate units. In order to compare these results quantitatively with the usual static approximation, it is easier to first make the static approximation [setting $\exp(\beta\omega)=1+\beta\omega$] before performing the k_1,k_2 integrals. In Figs. (16a) and (17a), we have done so for σ_{xx} and σ_{zz}, and it is readily apparent that the static approximation for σ_{xx} is about as accurate as for the specific heat and the perpendicular ($\theta=0$) SFD, indicating that the apparent power law in the experimentally accessible regime (outside the region of the T_c distribution) is more negative than in the static limit. The static approximation is much better for σ_{zz}, but the small overall magnitude of this quantity (and the rising background as T decreases) probably makes it difficult to observe quantitatively. Also, if one attempts to fit the high temperature region based upon the Maki-Thompson 2D limit, it is imperative that one correctly subtract the Aslamazov-Larkin contribution pictured here. In Figs. (16b) and (17b), we have presented log-log plots of σ_{xx}/T and σ_{zz}/T versus $\ln(T/T_c)$ for $\xi_{ab}(0)=10$ and 20 Å, respectively. Note that these curves do not scale with $C^+(T)$ or $\chi_{zz}(T)/T$, except for certain values of the parameters.

In fits to experimental data, it is important to note that recent measurements[27] of the SFD and the ^{63}Cu NMR linewidth[3,4] have indicated a decrease in the normal-state susceptibility as T_c is approached from above. As spin-flip scattering is expected to be important in normal-state conductivity of the copper oxides, one should find some procedure of determining the precise T dependence of the normal state ρ_{ij}. Perhaps by measuring the fluctuation magnetoconductivity for $\mathbf{B}\|\hat{\mathbf{c}}$ and $\mathbf{B}\perp\hat{\mathbf{c}}$, and subtracting those results, one might be able to determine the correct T dependence of the background. A recent calculation of the fluctuation magnetoconductivity for $\mathbf{B}$ in these directions has been presented.[31] In that calculation, the authors expanded about T_{c0} instead of $T_c(B)$, dropping the orbital term for $\mathbf{B}\perp\hat{\mathbf{c}}$, which is quadratic in B to leading order in $T-T_{c0}$, but linear in B to leading order in $T-T_c(B)$. A numerical evaluation[46] for $\mathbf{B}\|\hat{\mathbf{c}}$ has been performed, which shows a nearly linear B dependence near to T_{c0}. In addition, they considered only the $N=1$ case. They also neglected the dynamics, which should greatly alter the Maki-Thompson terms well above $T_c(B)$. More important, Patton[47] showed that in condensing into the superconducting state, the normal quasiparticles attain a lifetime that vanishes as $T\to T_c$, removing the divergence of the Maki-Thompson diagrams (and hence the necessity for introducing a τ_ϕ). These may be some of the reasons those authors inferred $\tau_\phi k_B T_c/h\sim 1.3$, a value we believe is at least a factor of $\gtrsim 5$ too low for the Y-Ba-Cu-O sample measured, which had an anomalously low T_{c0} of 85.5 K. If their value were correct, it would likely imply a large contribution to $1/\tau_\phi$ from a homogeneous mechanism, which would not be relevant to the observability of the high-field regime.

VII. DISCUSSION AND CONCLUSIONS

We have presented a model for the superconducting properties of the copper oxide materials which differs from previous models in that it properly takes account of the multiplicity of superconducting layers per unit cell. For most properties near to T_c, this feature does not make too much of a difference, but the addition of the higher pair bands can make a substantial contribution to the fluctuations well above T_c. The degree to which the upper bands are important depends not only upon the γ value, but also upon the $\xi_{ab}(0)$ value [from Eq. (29b)]. The smaller the $\xi_{ab}(0)$ value, the more important the contributions from the upper bands.

In addition, we have demonstrated explicitly that dynamic effects are essential, if one is to properly treat the temperature regime far from T_c. Even in the 3D regime near to T_c, the inclusion of the dynamics appears to alter the apparent divergence of the fluctuation quantities from the classic static result ($|T-T_c|^{-1/2}$). Hence, fits based upon the assumption of this simple power law in the Gaussian regime should be modified.

The most important result presented here is the prediction of oscillations in the angular dependence of the high-field SFD. Although we have not shown it explicitly, one would also infer that a measurement of the angular dependence of the high-field magnetoresistance in the Gaussian fluctuation regime should also exhibit Shubnikov-de Haas-like oscillations. These oscillations are intrinsic to the layered structure of the superconducting materials, arising from multiple degenerate minima present in the periodic potential for $\mathbf{B}\perp\hat{\mathbf{c}}$. In order to observe these oscillations, it is necessary to have $\omega_c\tau_\phi\gtrsim 1$, which should be true in the best samples (with $\tau_\phi k_B T_c/\hbar\gg 1$) for fields in the range 10–50 T. In addi-

tion, it is necessary that q_c^* be sufficiently large in the angular region $\pi/4<\theta<\pi/2$ that the oscillations do not become eliminated. This condition is most likely to be met for materials with $N\geq 2$. We believe that for Y-Ba-Cu-O, the parameters are likely to be such that at least one peak in the high-field SFD should be observable.

We reiterate that the angular dependence of the high field $\chi_B(\theta,T)$ at fixed T is predicted to differ greatly from that at low fields. The weak field $\chi_{\rm eff}(\theta,T)$ obeys a simple, "anisotropic mass" form in the 3D regime above T_c, which is closely related to the $H_{c2}(\theta)$ in the 3D regime below T_c. The strong field $\chi_B(\theta,T)$ does not behave in this manner, because it contains contributions from degenerate absolute minima in the potential, whereas H_{c2} only depends upon the value (not the degeneracy) of the lowest eigenvalue. Hence, in the 3D regime, one merely has

$$H_{c2}=\phi_0/[2\pi\xi_{ab}^2(T)a_0(\theta,0)] ,$$

the usual anisotropic form.[34] Similarly, the anisotropy of H_{c1} in the 3D regime only depends upon the effective mass ratio, although the precise form[34] of the angular dependence is more complicated than that of H_{c2}.

ACKNOWLEDGMENTS

The author would like to acknowledge useful discussions with J. R. Clem, V. J. Emery, D. C. Johnston, D. F. Finnemore, R. Fuchs, B. N. Harmon, V. G. Kogan, and K. Machida. He received some correspondence from N. Goldenfeld, S. Renn, and J. Annett, confirming (subsequent to his derivation) Eqs. (2), (3), and (7). He is particularly indebted to D. C. Johnston for innumerable lengthy discussions on these topics. He has also had a great deal of assistance from W. C. Lee in preparing the figures. He would like to thank B. N. Harmon, D. C. Johnston, and especially R. Fuchs for critical readings of the manuscript. Finally, the author would like to express his appreciation to the entire solid-state group of Iowa State University, who have kindly allowed him extended use of the majority of the VAX workstations during the past several months in order to perform these calculations. The Ames Laboratory is operated for the U. S. Department of Energy by Iowa State University under Contract No. W-7405-ENG-82. This work was supported by the Director for Energy Research, Office of Basic Energy Sciences.

APPENDIX

In this appendix, we demonstrate that Eqs. (11) and (12) of the text hold rigorously for an arbitrary magnetic field strength and direction, for the special case $N=2$. Using the Fourier transform for ψ_{jn} in terms of ψ_{kzn}, the Gaussian free energy may be written as

$$F_S-F_N=C\sum_{k_z}\int d^2\mathbf{r}F_{12} , \tag{A1a}$$

where

$$F_{12}=\psi_{k_z1}^*(H_0+\varepsilon_2)\psi_{k_z1}+\psi_{k_z2}^*(H_0+\varepsilon_2)\psi_{k_z2} +\psi_{k_z1}^*|\gamma|e^{-i\eta}\psi_{k_z2}+\psi_{k_z2}^*|\gamma|e^{i\eta}\psi_{k_z1} , \tag{A1b}$$

where $|\gamma|e^{-i\eta}\equiv\gamma_2+\gamma_1^*$, and C is an unimportant constant. Note that $|\gamma|$ and η depend upon position in the presence of a magnetic field.

Letting

$$\psi_{k_z1}=e^{-i\eta/2}(\tilde\psi_{k_z1}+\tilde\psi_{k_z0})/\sqrt{2} \tag{A2a}$$

and

$$\psi_{k_z2}=e^{+i\eta/2}(\tilde\psi_{k_z1}-\tilde\psi_{k_z0})/\sqrt{2} , \tag{A2b}$$

we have

$$F_{12}=\tfrac{1}{2}\{e^{i\eta/2}(\tilde\psi_{k_z1}^*+\tilde\psi_{k_z0}^*)[(H_0+\varepsilon_2)(\tilde\psi_{k_z1}+\tilde\psi_{k_z0}) +|\gamma|(\tilde\psi_{k_z1}-\tilde\psi_{k_z0})]e^{-i\eta/2} +e^{-i\eta/2}(\tilde\psi_{k_z1}^*-\tilde\psi_{k_z0}^*)[(H_0+\varepsilon_2)(\tilde\psi_{k_z1}-\tilde\psi_{k_z0}) +|\gamma|(\tilde\psi_{k_z1}+\tilde\psi_{k_z0})]e^{i\eta/2}\} . \tag{A3}$$

We now define

$$(H_0+\varepsilon_2+|\gamma|)\tilde\psi_{k_z1}\equiv\tilde E_{k_z1}\tilde\psi_{k_z1}$$

and

$$(H_0+\varepsilon_2-|\gamma|)\tilde\psi_{k_z0}\equiv\tilde E_{k_z0}\tilde\psi_{k_z0} , \tag{A4}$$

consistent with Eq. (12b) for $\delta\tilde\lambda_n=0$.

We then obtain

$$F_{12}=\tfrac{1}{2}[e^{i\eta/2}(\tilde\psi_{k_z1}^*+\tilde\psi_{k_z0}^*)(\tilde E_{k_z1}\tilde\psi_{k_z1}+\tilde E_{k_z0}\tilde\psi_{k_z0})e^{-i\eta/2} +e^{-i\eta/2}(\tilde\psi_{k_z1}^*-\tilde\psi_{k_z0}^*)(\tilde E_{k_z1}\tilde\psi_{k_z1}-\tilde E_{k_z0}\tilde\psi_{k_z})e^{i\eta/2}] \tag{A5a}$$

$$=\sum_{n=0}^{1}\tilde E_{k_zn}|\tilde\psi_{k_zn}|^2 , \tag{A5b}$$

which is Eq. (11) of the text. We note that we have dropped terms arising from H_0 operating on η, some of which are non-Hermitian. These terms are nonvanishing, and in the preceding formalism, would also cause the diagonalization procedure to fail. The diagonalization procedure can be made exact, and F_{12} made Hermitian, however, by the following procedure: From Eq. (1) of the text, we integrated by parts to obtain terms such as $\psi_{k_z1}^*H_0\psi_{k_z1}$, with H_0 operating to the right. We could instead have integrated by parts the other way, obtaining H_0 operating to the left. By symmetrizing, we obtain $H_0=\frac{1}{2}(H_{0R}+H_{0L})$, where H_{0R} and H_{0L} are of identical form, but operate to the right and left, respectively. Note that for the choice of gauge given in the text, $\nabla\eta\cdot\mathbf{A}=0$. These three procedures differ by surface terms only. We now let

$$\tilde\psi_{k_z1}=|\tilde\psi_{k_z1}|e^{i\chi_1},\tilde\psi_{k_z0}=|\tilde\psi_{k_z0}|e^{i\chi_0} .$$

The diagonalization procedure can be made exact by choosing $\chi_1=\chi_0$ and

$$\sum_{\mu=1,2} (\partial_\mu \eta)(\partial_\mu \chi_0)/m_\mu = 0 \ . \tag{A6}$$

For the choice of gauge given in the text, this implies χ_0 is independent of y. It is then easy to show that the fully diagonalized Hamiltonian becomes

$$\tilde{H}_n = H_0 + \bar{\lambda}_n + \delta\bar{\lambda}_n \ , \tag{A7}$$

where

$$\delta\bar{\lambda}_n = \sum_{\mu=1,2} (\partial_\mu \eta)^2/8m_\mu \ . \tag{A7'}$$

For the choice of gauge given in the text, we have

$$\delta\bar{\lambda}_n = \frac{(2eB\sin\theta)^2[\zeta_1 d(\zeta_1+\zeta_2\cos q)-\zeta_2 d'(\zeta_2+\zeta_1\cos q)]^2}{8m_2(\zeta_1^2+\zeta_2^2+2\zeta_1\zeta_2\cos q)^2} \ , \tag{A8}$$

which has the same form for both $n=0$ and $n=1$. We note that $\delta\bar{\lambda}_n \to 0$ for $B\sin\theta \to 0$, and for the special case $\zeta_1=\zeta_2$ and $d=d'$, so that this complication does not arise for $N=1$. However, even in the case $\zeta_1=\zeta_2$ (but $d\neq d'$), this term does not vanish, except at $\theta=0$. $\delta\bar{\lambda}_n$ is well behaved for all q values.

A microscopic calculation reveals that $\delta\bar{\lambda}_n(q=0)$ can be removed by a shift in the Fermi energy, so one should really replace $\delta\bar{\lambda}_n(q)$ by

$$\delta\tilde{\lambda}_n(q) = \delta\bar{\lambda}_n(q) - \delta\bar{\lambda}_n(q=0) \ .$$

Hence, the eigenvalues obtained by neglecting $\delta\tilde{\lambda}_n(q)$ are exact to $O(B^2\sin^2\theta)$. $\delta\tilde{\lambda}_n$ will cause a reduction in T_c (for $\theta\neq 0$) of order B^3, which *counteracts* but does not eliminate the upward curvature arising from dimensional crossover in H_{c2} for $\theta\neq 0$. We note that the regime of the fluctuation diamagnetism will not be affected by $\delta\tilde{\lambda}_n$. The region of the high-field regime we have considered here (with eigenvalues linear in B) will also not be affected, except that $\delta\tilde{\lambda}_n$ removes the degeneracies at the special θ_m values [Eq. (17)], (unless $\zeta_1 d=\zeta_2 d'$ for $n=0$) weakening slightly the amplitude of the oscillations in $\chi_B(\theta)$. At these special angles, the smearing of the maxima will be greater for $n=1$ than for $n=0$.

This derivation is easily generalized to the case of single-particle propagation in a two layer system, using second quantization. That procedure leads to a microscopic derivation of Eq. (1), which will be presented elsewhere. It is straightforward, though very tedious, to generalize this procedure to arbitrary N.

*Present address: Solid State Division, Oak Ridge National Laboratory, Oak Ridge, TN 37831-6032.

[1]Y. Uemura *et al.*, J. Phys. (Paris) Colloq. **8**, C49-2087 (1988).

[2]S. Mitra *et al.*, Bull. Am. Phys. Soc. **34**, 1014 (1989); Phys. Rev. B **40**, 2674 (1989).

[3]Y. Kitaoka *et al.* (unpublished); P. Wzietek *et al.*, Europhys. Lett. **8**, 363 (1989).

[4]M. Takigawa *et al.* (unpublished); P. C. Hammel *et al.*, Bull. Am. Phys. Soc. **34**, 1011 (1989).

[5]A. J. Sievers, Bull. Am. Phys. Soc. **33**, 507 (1988).

[6]J. Orenstein, Bull. Am. Phys. Soc. **34**, 925 (1989).

[7]R. A. Klemm, K. Scharnberg, D. Walker, and C. T. Rieck, Z. Phys. B **72**, 139 (1988).

[8]Hoydoo You *et al.*, Phys. Rev. B **38**, 9213 (1988).

[9]N. Nücker *et al.*, Phys. Rev. B **37**, 5158 (1988).

[10]C. Stassis *et al.* (unpublished).

[11]G. Shirane *et al.*, Phys. Rev. Lett. **59**, 1613 (1987).

[12]A. Arko *et al.*, Bull. Am. Phys. Soc. **34**, 809 (1989); and (unpublished).

[13]S. Martin *et al.*, Phys. Rev. Lett. **60**, 2194 (1988).

[14]A. Thompson, Solid State Commun. **13**, 1911 (1973).

[15]B. Oh *et al.*, Phys. Rev. B **37**, 7861 (1988); T. A. Friedman, J. P. Rice, and D. M. Ginsberg (unpublished).

[16]S. E. Inderhees *et al.*, Phys. Rev. Lett. **60**, 1178 (1988); Bull. Am. Phys. Soc. **34**, 843 (1989).

[17]K. Kanoda *et al.*, J. Phys. Soc. Jpn. **57**, 1554 (1988).

[18]W. Lawrence and S. Doniach, in *Proceedings of the Twelfth International Conference on Low Temperature Physics*, edited by Eizo Kanda (Academic, Kyoto, Japan, 1971), p. 361.

[19]U. Welp *et al.*, Phys. Rev. Lett. **62**, 1908 (1989).

[20]R. A. Klemm, M. R. Beasley, and A. Luther, Phys. Rev. B **8**, 5072 (1973).

[21]R. R. Gerhardts, Phys. Rev. B **9**, 2945 (1974).

[22]J. Gollub, M. R. Beasley, and M. Tinkham, Phys. Rev. Lett. **25**, 1646 (1970); Phys. Rev. B **7**, 3039 (1973).

[23]R. A. Klemm, A. Luther, and M. R. Beasley, Phys. Rev. B **12**, 877 (1975); R. A. Klemm, Ph.D. thesis, Harvard University (1974).

[24]Y. Tokura, H. Takagi, and S. Uchida (unpublished); J. T. Markert and M. B. Maple (unpublished).

[25]See, for example, C. Kittel, *Introduction to Solid State Physics*, 3rd ed. (New York, Wiley, 1968), pp. 148–150.

[26]L. C. Smedskjaer *et al.*, Physica **156C**, 269 (1988).

[27]W. C. Lee, R. A. Klemm, and D. C. Johnston, Phys. Rev. Lett. **63**, 1012 (1989).

[28]N. W. McLachlan, J. Math. Phys. **25**, 209 (1946). See the figure on p. 223.

[29]C. Van Tendeloo, H. W. Zandbergen, and S. Amelinckx, Solid State Commun. **63**, 389 (1987); M. M. Fang *et al.*, Phys. Rev. B **37**, 2334 (1988); D. F. Finnemore (private communication).

[30]A. Schmid, Phys. Rev. **180**, 527 (1969).

[31]A. G. Aronov, S. Hikami, and A. I. Larkin, Phys. Rev. Lett. **62**, 965 (1989). Note that the τ_ϕ inferred by these authors included possible contributions arising from homogeneous pair breaking, which would not affect the high-field regime discussed here.

[32]N. P. Ong *et al.*, Physica **153-155C**, 1072 (1988).

[33]J. Kurkijärvi, V. Ambegaokar, and G. Eilenberger, Phys. Rev. B **5**, 868 (1972).

[34]R. A. Klemm and J. R. Clem, Phys. Rev. B **21**, 3890 (1980); R. A. Klemm, *ibid.* **38**, 6641 (1988); **41**, 117 (1990).

[35]H. Schmidt, Z. Phys. **216**, 336 (1968).

[36]K. Maki and N. Takayama, J. Low Temp. Phys. **5**, 313 (1971); K. Maki, Phys. Rev. Lett. **30**, 648 (1973).

[37]Y. Yeshurun *et al.*, Phys. Rev. B **38**, 11 828 (1988).

[38]D. E. Farrell *et al.*, Phys. Rev. Lett. **61**, 2805 (1988).

[39]A. Malozemoff *et al.*, Phys. Rev. B **38**, 7203 (1988).

[40]L. G. Aslamazov and A. I. Larkin, Fiz. Tverd. Tela (Leningrad) **10**, 1104 (1968).

[41]K. H. Quader and E. Abrahams, Phys. Rev. B **38**, 11978 (1988).

[42]D. J. Scalapino, M. Sears, and R. A. Ferrell, Phys. Rev. B **6**, 3409 (1972).
[43]B. Mühlschlegel, Z. Phys. **155**, 313 (1959).
[44]R. P. Sharma *et al.*, Phys. Rev. B **38**, 9287 (1988).
[45]K. Maki, Prog. Theor. Phys. **39**, 897 (1968); **40**, 193 (1968); R. S. Thompson, Phys. Rev. B **1**, 327 (1970).
[46]C. T. Rieck, T. Wölkhausen, D. Fay, and L. Tewordt, Phys. Rev. B **39**, 278 (1989).
[47]B. R. Patton, Phys. Rev. Lett. **27**, 1273 (1971).